Lab on a Chip

CRITICAL REVIEW

View Article Online
View Journal | View Issue

Cite this: *Lab Chip*, 2026, **26**, 1394

Microcavity-assisted microfluidic physical sensors: materials, structures, and multifunctional applications

Xinyi Qu,[ab] Jianfeng Ma,[ab] Degong Zeng,[ab] Jinan Luo,[ab] Jingzhi Wu,[ab] Chuting Liu,[ab] Zhikang Deng,[ab] Lvjie Chen,[ab] Rongkuan Han,[ab] Yancong Qiao *[ab] and Jianhua Zhou *[ab]

Received 27th August 2025,
Accepted 28th September 2025

DOI: 10.1039/d5lc00822k

rsc.li/loc

Microfluidic sensing has long been dominated by chemical approaches that usually rely on fluorescent labels or specific reagents to achieve high specificity. However, these methods often require complex preparation and suffer from limited real-time capability, challenges that become more pronounced in wearable and portable platforms. In contrast, physical sensing offers a complementary route by detecting variations in mechanical, acoustic, optical, or thermal properties directly, enabling label-free, faster, and more robust operation. Under this background, microcavity architectures stand out as one promising option among various physical sensing designs. By spatially confining and enhancing physical signals at the miniature scale, microcavities can sharpen detection resolution and extend dynamic range. These gains are further elevated through the use of tailored materials and are reinforced by fabrication strategies that deliver precise geometry control and adaptable functionality. Harnessing such features, microcavity-based systems have been leveraged in fields ranging from high-resolution tactile sensing in soft robotics to wearable healthcare and human-machine interaction. This review surveys recent progress in materials, fabrication methods, and sensing mechanisms for microcavity-assisted microfluidic physical sensors, and discusses future directions toward broader adoption and scalable deployment.

[a] *Key Laboratory of Sensing Technology and Biomedical Instruments of Guangdong Province, School of Biomedical Engineering, Shenzhen Campus of Sun Yat-sen University, Shenzhen, 518107, China. E-mail: qiaoyc3@mail.sysu.edu.cn, zhoujh33@mail.sysu.edu.cn*

[b] *Key Laboratory of Sensing Technology and Biomedical Instruments of Guangdong Province, School of Biomedical Engineering, Sun Yat-sen University, Guangzhou, 510275, China*

Introduction

With the rapid advancement of micromachining technology and micro/nano-scale manufacturing processes, microfluidic technology has progressively emerged as an indispensable key technology in the biomedical field, owing to its remarkable advantages, such as high throughput,[1] minimal sample

Xinyi Qu

Xinyi Qu received her Bachelor's degree from the School of Biomedical Engineering at Southern Medical University (Guangzhou, China), and she is now continuing her studies towards a Master's degree at Sun Yat-sen University (Shenzhen, China). Her current research focuses on the development of micro/nano fabrication technology and microcavity-assisted physical sensors.

Jianfeng Ma

Jianfeng Ma received his Bachelor's degree from the School of Biomedical Engineering at Guangzhou Medical University (Guangzhou, China), and he is now continuing his studies towards a Master's degree at Sun Yat-sen University (Shenzhen, China). His current research focuses on the application of flexible sensor system in sleep monitoring.

consumption,[2] rapid analysis,[3] and precise control.[4] Microfluidic chips are capable of integrating complex experimental procedures into miniaturized devices while substantially enhancing detection efficiency and accuracy,[5] thereby demonstrating immense potential in disease diagnosis,[6] drug screening,[7,8] and biomolecular analysis.[9,10]

In microfluidic sensing systems, chemical or biological sensing approaches represent the predominant sensing mechanisms, typically depending on fluorescent markers or specific reagents.[11–13] By contrast, microfluidic sensing approaches based on physical principles have garnered increasing attention from researchers in recent years, due to their label-free nature, rapid response, and high stability, and have achieved substantial progress in wearable devices,[14,15] flexible electronics,[16] and biomedical engineering.[17] Physical sensing techniques, such as mechanical,[14] acoustic,[18] optical,[19] and thermal sensing,[20] enable real-time, highly sensitive, and non-invasive detection by directly monitoring the physical properties or state changes of substances within fluids.

In microfluidic chips, the design of functional architectures determines the system's manipulation precision and signal transduction efficiency. Consequently, researchers have progressively developed various active or semi-active components to meet diverse application needs, such as flexible diaphragms for fluid regulation,[21] magnetic/electric valves for flow path switching,[22,23] and micropillar arrays to enhance the reaction interface.[24] While these structures offer distinct advantages across specific application scenarios, in the trend of pursuing higher sensitivity, faster response times, and increased wearability, they struggle to simultaneously meet these demands. Under this backdrop, microcavity structures, capable of significantly enhancing signals at the micro and nanoscale, are increasingly attracting scholarly attention. A microcavity is a closed or semi-closed structure that can effectively confine and enhance optical, acoustic, and mechanical signals at the miniature scale.[25,26] Owing to its spatial confinement characteristics,[19] the microcavity enhances the detection system's responsiveness to weak signals and demonstrates unique advantages in improving the sensitivity, response speed, and detection limit of physical signal sensing. In particular, sealed airbag-based microcavity structures with active pressurization capabilities offer enhanced mechanical tunability and conformal skin-sensor interaction, enabling continuous and controllable signal output, which is highly advantageous for physiological signal acquisition and multimodal wearable sensing.[27]

The integration of microcavity structures with microfluidic sensing technology further extends the functionality and application scope of microfluidic chips. Currently, microcavity-assisted microfluidic sensing shows a diversified trend in both material architectures and functional implementation, encompassing lightweight, high specific-surface-area (SSA) cavities based on porous polymers[28] or carbon materials,[29] microchannels with self-healing liquid metal (LM) capable of dual-mode electrical and mechanical response,[30,31] electret membrane cavities with prolonged charge retention,[32] and closed/semi-closed polymeric cavities.[33] These architectures not only improve sensitivity and dynamic range in mechanical sensing *via* active pressurization or passive resonance, but also facilitate efficient thermoacoustic and electroacoustic conversion in acoustic transduction, and enhance photothermal coupling efficiency in optical and thermal modalities. In addition, certain microcavities function as patterned encapsulation layers, or utilize microfluidic platforms as tools to assist in sensor assembly and scalable manufacturing.[34] Consequently, they empower wearable healthcare systems with physiological signal monitoring;[35,36] equip flexible robotic and human-machine interaction (HMI) end-effectors

Yancong Qiao

Yancong Qiao is an associate professor in the School of Biomedical Engineering at Sun Yat-sen University (Shenzhen, China). He received his B.S. degree from the Department of Electronic Science and Technology of Xi'an Jiaotong University in 2016 and his Ph.D. degree from the School of Integrated Circuits of Tsinghua University in 2021. His current research interests focus on flexible MEMS systems, biomedical micro/nano sensing, flexible electronic skins, and systems, soft robot, as well as neuromimics and intelligent physiological signal analysis, soft robots, etc.

Jianhua Zhou

Jianhua Zhou is a full professor in the School of Biomedical Engineering at Sun Yat-sen University (Guangzhou, China). He received his Ph.D. in chemistry from Hong Kong University of Science and Technology. He was a visiting scholar at Harvard University, Queen's University (Kingston, Canada), and Swansea University (Wales, UK). His research interests are in a wide range of in vitro diagnosis (IVD) and rapid detection, microfluidic technology, biological/chemical sensing, advanced micro/nano processing technology, wearable sensing and human-machine interface, AI-assisted high throughput technology, Image-mediated diagnosis and treatment, artificial organs and regenerative medicine, etc.

with multimodal tactile perception and touchless recognition;[37,38] and enable ultra-wide-range sensing,[39] acoustic communication,[18] and optoelectronic multifunctional detection for environmental and industrial monitoring.[40] Fig. 1 provides an overview of the key materials and manufacturing processes of microcavity-assisted microfluidic physical sensors, along with their functional roles across diverse application domains. However, existing technologies face challenges such as high integration complexity, limited material options, insufficient long-term stability, and inadequate reusability. Consequently, systematically investigating the design principles, material selection, and performance optimization methods of microcavity-assisted microfluidic physical sensing holds significant scientific importance and practical application value.

This review focuses on microcavity-assisted physical sensors from three perspectives: material selection, structural design, and application cases. It systematically discusses the

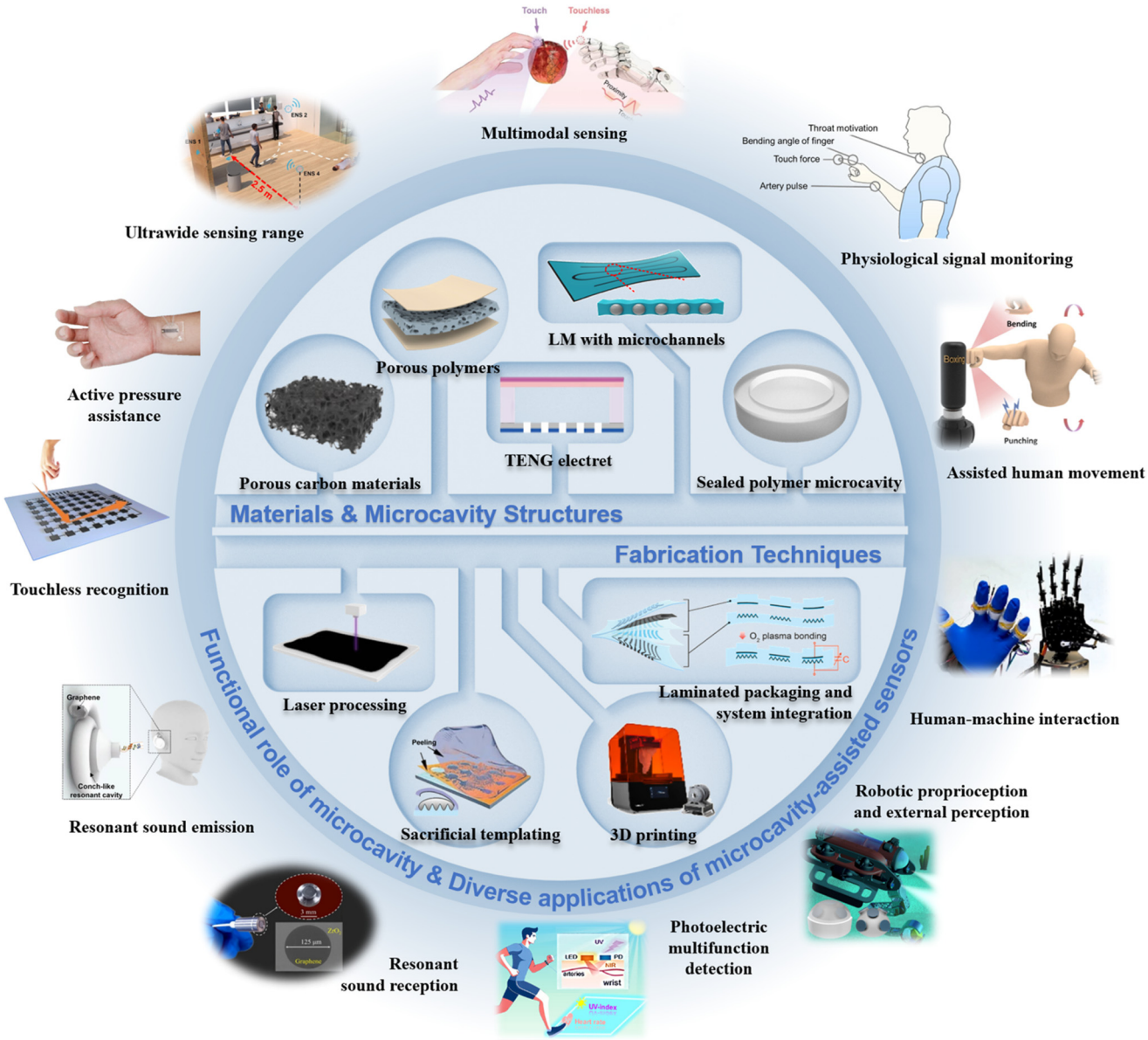

Fig. 1 Schematic of the materials, fabrication, and diverse applications of microcavity-assisted microfluidic physical sensors. It covers porous polymer and carbon-based materials, liquid metal microchannel architectures, electret-based membranes, and sealed polymer cavities, illustrating their functional roles in augmenting mechanical, acoustic, optical, and thermal transduction, along with the corresponding fabrication methodologies, and presenting representative application domains, including wearable healthcare monitoring, HMI technologies, and environmental monitoring. Reproduced with permission from ref. 15. Copyright (2024) Elsevier, ref. 28. Copyright (2023) Wiley-VCH GmbH, ref. 29. Copyright (2025) AAAS, ref. 30. Copyright (2025) Wiley-VCH GmbH, ref. 32. Copyright (2024) Elsevier, ref. 35. Copyright (2024) Springer Nature, ref. 37. Copyright (2024) American Chemical Society, ref. 39. Copyright (2023) American Chemical Society, ref. 46. Copyright (2024) Wiley-VCH GmbH, ref. 49. Copyright (2024) Springer Nature, ref. 50. Copyright (2023) Springer Nature, ref. 51. Copyright (2024) American Chemical Society, ref. 58. Copyright (2024) American Chemical Society, ref. 96. Copyright (2023) American Chemical Society, and ref. 97. Copyright (2025) American Chemical Society.

critical role of microcavity structures in enhancing sensing performance and optimizing detection principles. Specifically, the application of microcavities in biomedical detection is emphasized comprehensively, aiming to provide valuable references and guidance for the design and development of microfluidic physical sensors. Therefore, the structure of the subsequent chapters is organized as follows: chapter 2 concentrates on the materials and fabrication principles of microcavity sensors, providing a systematic review of flexible polymers, LMs, carbon-based nanomaterials, and other functional material systems. It also analyzes how fabrication strategies, including laser processing, sacrificial templating, 3D printing, and laminated encapsulation, precisely define cavity geometries, enhance mechanical robustness, and facilitate scalable integration. Chapter 3 elucidates the device-level coupling between microcavity architectures and sensing mechanisms. It begins by analyzing how structural elements enable high gain, energy autonomy, and multimodal outputs within resistive, capacitive, and triboelectric modalities. Subsequently, it examines acoustic transduction, highlighting how different cavities enhance gain in thermoacoustic and electroacoustic conversion. The discussion then extends to optical and thermal domains. Chapter 4 summarizes current challenges in long-term stability, high-throughput fabrication, and intelligent data integration, and looks ahead to the development directions and application prospects of microcavity technology in wearable healthcare, HMI, environmental monitoring, and extreme condition sensing.

Materials and fabrication strategies

Microcavity structures enhance target physical signals by spatially confining acoustic, photonic, thermal, or mechanical fields. The design of flexible materials, as well as the integration of multifunctional material systems, governs the microcavity's dimensional precision, operational robustness, and functional versatility. Thus, materials engineering and fabrication methodologies remain fundamental to advancing research on microcavity-assisted physical sensing technologies. This section systematically reviews material classifications and representative fabrication techniques.

Materials

Polymers. Polymers are widely used as microcavity wall materials or sensing layers, due to their flexibility, processability, and biocompatibility. Typical polymer candidates include silicone elastomers, such as polydimethylsiloxane (PDMS)[41] and Ecoflex,[35] thermoplastic polyurethane (TPU),[42,43] engineering plastics like polyimide (PI)[35] and polyethylene terephthalate (PET),[32] fluorinated polymers, such as polytetrafluoroethylene (PTFE)[36] and perfluoroalkoxy alkane (PFA),[36] as well as biocompatible hydrogels including polyvinyl alcohol (PVA).[31] Elastomers, such as TPU/PDMS enable the mass production of multicavity arrays at low temperatures through fully printed processes, allowing real-time monitoring of pulse and blood pressure in wearable applications (Fig. 2a).[27] Porous PDMS-Ag composite sponges are fabricated using sacrificial template molding, with controllable pore size and uniformly embedded silver particles, achieving a pressure sensitivity of up to 0.047 kPa^{-1} (Fig. 2b).[41] Guo *et al.* directly employ carbon black (CB) as a photothermal absorber and glucose as a porogen to produce porous PDMS membranes (Fig. 2c).[44] Building on previous work, Liao *et al.* fabricate composite materials with tunable pore size distribution by varying the proportion of carbon nanotube (CNT)/TPU conductive sponge and chemical foaming silicone rubber (SR). The hierarchical porous architecture incorporates a "macro-pore energy storage and micro-pore sensing" cavity design, which significantly broadens both the sensing range and sensitivity (Fig. 2d).[42] These porous or layered polymeric materials are frequently integrated with energy-autonomous mechanisms. For instance, embedded triboelectric units impart self-powering functionality to the devices, and when paired with machine learning algorithms, support applications such as rehabilitation assessment.[45] Furthermore, biomimetic multimodal self-powered tactile skins achieve high intrinsic piezoresistive sensitivity by incorporating carbon nanoparticles (CNs) into porous fluororubber/TPU composite sponges.[43] The combination of microcavities, hierarchical porosity, and low Young's modulus imparts high sensitivity to polymer-based sensors.

Liquid metals. Room-temperature LMs exhibit exceptional electrical conductivity, fluidic reconfigurability, and intrinsic self-healing capability, rendering them ideal for the construction of flexible and stretchable microcavity-based circuits. Gallium-based alloys, such as EGaIn and Galinstan are the most commonly employed in these devices. Their ability to fill and dynamically reshape microcavities in response to external mechanical stimuli makes them highly suitable as core sensing elements in wearable sensors, including electronic skin systems. Researchers have investigated LMs configured into microchannels of various geometries. Zhao *et al.* inject LM into microchannels with distinct shapes and demonstrate that spiral geometries enhance pressure sensitivity, while wavy geometries show greater responsiveness to tensile deformation (Fig. 3a).[31] Li *et al.* fabricate an embedded liquid metal microelectrode (LM-ME) array that maintains uniform strain distribution across curved surfaces, thereby enabling three-dimensional pressure mapping (Fig. 3b).[46] Several studies further integrate LM with functional materials. To improve wearing comfort, Xu *et al.* develop a highly breathable LM foam by integrating porous PDMS and LM, enabling real-time monitoring of human physiological signals (Fig. 3c).[47] Conductive polymer/LM composite electrodes with autonomous self-healing and electrical restoration capabilities provide both mechanical resilience and energy-autonomous performance.[48] LM-based triboelectric microcavity structures are also extended to demanding applications, such as underwater gripping, deep-sea pressure sensing,[49] and scalable printable boxing training patches.[50] LMs are promising candidates for constructing stretchable microcavity-based circuits and multimodal sensing architectures, particularly in the domains of flexible electronics, pressure mapping, and self-healing sensor technologies.

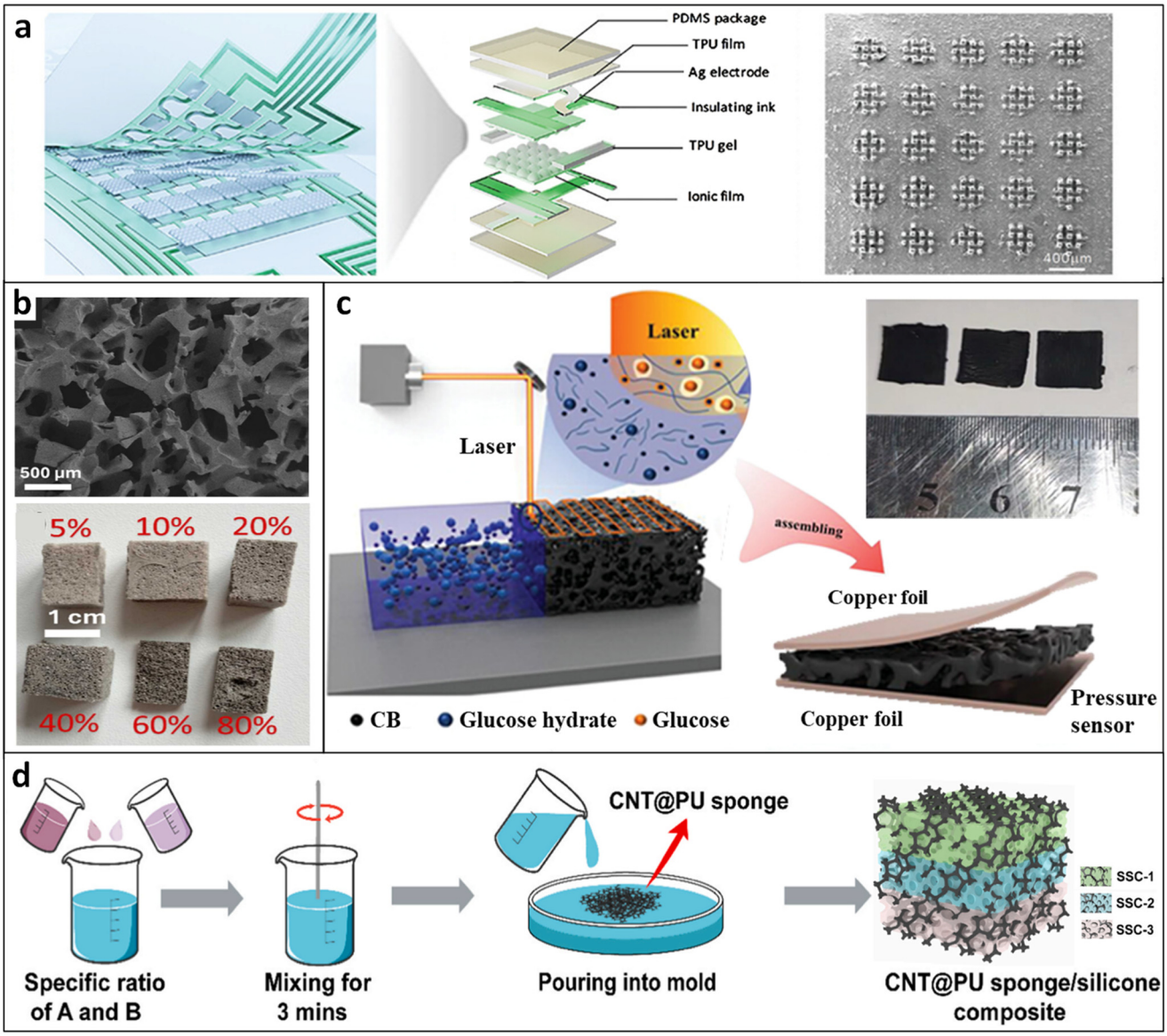

Fig. 2 Polymer materials for constructing cavity walls and porous sensing layers. a. Exploded view and SEM image of the fully printed sensor array. TPU acts as a spacer layer, providing mechanical support to both the top and bottom surfaces of the sensor. PDMS encapsulation isolates the device from air exposure, thereby preventing oxidation of the electrodes and sensing layer.[27] Reproduced with permission from ref. 27. Copyright (2025) Wiley-VCH GmbH. b. SEM image of PDMS foam fabricated using a sacrificial template method, and optical photographs of PDMS foam doped with varying concentrations of silver nanosheets.[41] Reproduced with permission from ref. 41. Copyright (2025) Elsevier. c. Schematic illustration of the porous PDMS formation process and optical image of the porous sensing unit. CB absorbs heat from infrared laser irradiation, which initiates a cross-linking reaction in the PDMS precursor, resulting in solidification. Concurrently, laser-induced thermal decomposition of glucose hydrate generates steam, promoting the formation of internal pores within the PDMS matrix.[44] Reproduced with permission from ref. 44. Copyright (2023) Wiley-VCH GmbH. d. Fabrication process of CNT/PU conductive sponge. SR releases hydrogen gas during the foaming process, leading to pore formation within the conductive sponge. By adjusting the SR ratio, CNT/PU sponges with varying pore sizes and densities can be obtained.[42] A refers to the chemical blowing agent, and B refers to the curing agent, which are the two components of SR. Reproduced with permission from ref. 42. Copyright (2023) Elsevier.

Carbon materials. Graphene and CNTs, owing to their high SSA and superior electrical and thermal conductivities, are extensively employed in microcavity systems, primarily as functional sensing layers. Three-dimensional graphene foams serve as thermoacoustic loudspeakers, where cavity resonance significantly enhances thermoacoustic conversion, enabling sound emission levels up to 70 dB under 1 mm spacing and 1 W input power (Fig. 4a).[51] Spiral shell–shaped graphene microcavities further enable tunable acoustic amplification within the 1–10 kHz frequency band (Fig. 4b).[29] Graphene-based porous composite microcavities also serve as acoustic receiving elements. An ultralight graphene oxide (GO)/deoxyribonucleic acid (DNA) aerogel builds a tunable acoustic resonator within a 3D interconnected pore network,

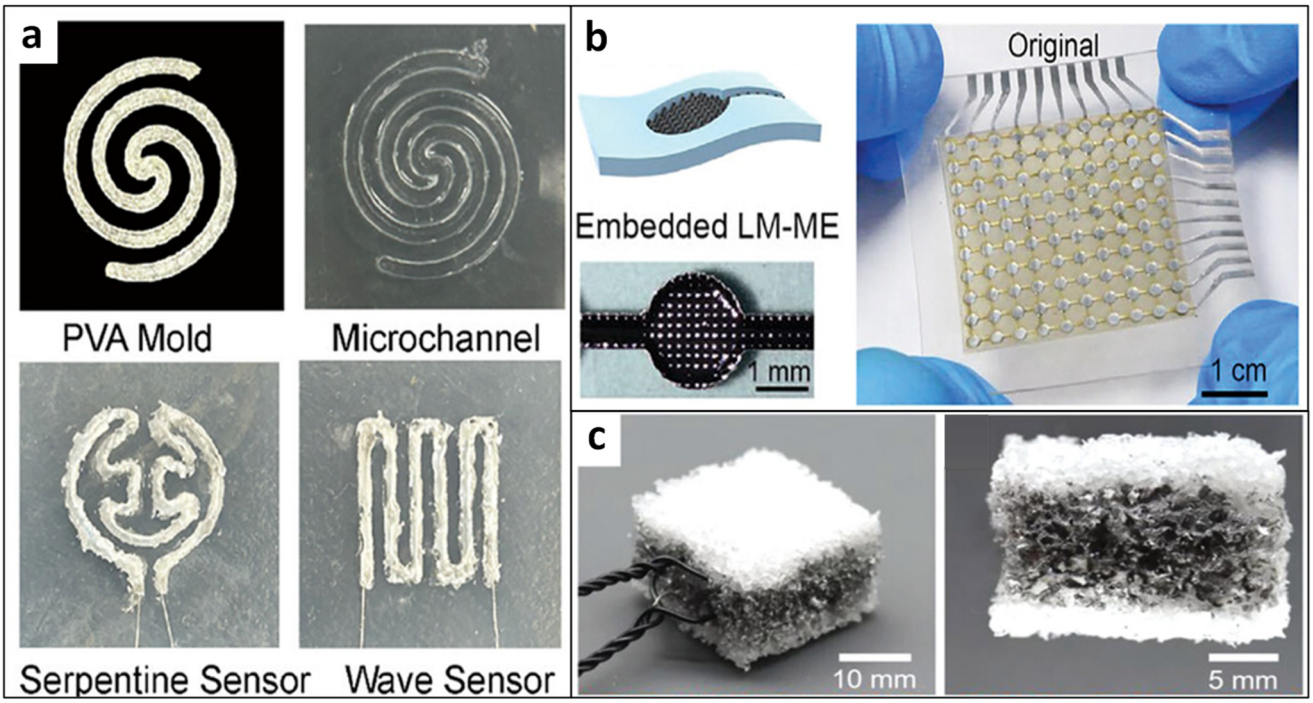

Fig. 3 LM sensing layers with diverse structural configurations. a. LM sensors with spiral, serpentine, and wave-shaped microchannels.[31] Reproduced with permission from ref. 31. Copyright (2025) Wiley-VCH GmbH. b. A schematic diagram and optical image of a single embedded LM-ME sensing unit, together with a digital photograph of the LM-ME array in its pristine state.[46] Reproduced with permission from ref. 46. Copyright (2024) Wiley-VCH GmbH. c. A photograph and side view of a breathable encapsulated LM foam-based soft stress sensor. The device consists of an integrated, delamination-free structure composed of PDMS foam in the top and bottom layers, and LM-coated PDMS foam in the middle layer.[47] Reproduced with permission from ref. 47. Copyright (2023) Wiley-VCH GmbH.

delivering a sensitivity of 74.4 kPa^{-1} to sound pressures above 68 dB across 300–4000 Hz while simultaneously resolving micro-pressures down to 0.31 Pa.[52] In addition, a sound-driven triboelectric nanogenerator (SD-TENG) fabricated by doping GO nanosheets into a polyvinylidene fluoride (PVDF) nanofiber membrane and integrating ring-shaped microcavity electrodes provides a voltage sensitivity of 4.76 V Pa^{-1} over 20–2000 Hz.[53] Superelastic graphene aerogels preserve their microcavity integrity and conductive networks across extreme temperature ranges (−196 °C to 300 °C), offering a pathway for harsh-environment sensing (Fig. 4c).[54] Composite configurations integrating graphene with other materials are engineered to optimize cavity performance. For instance, dome-like cavity arrays induced by pre-strained meshes in CNT-PDMS films result in uniform cavity distribution and suppress lateral strain interference (Fig. 4d);[55] closed graphene/poly(methyl methacrylate) (PMMA) microcavities function as miniature ultrasonic resonators (Fig. 4e);[56] silver–nitrogen–graphene (SNG) coupled resonators enable simultaneous refractive index, temperature, and pressure sensing (Fig. 4f);[57] and optical microcavities formed from pentaerythritol tetraacrylate (PETA) polymer and GO composites exhibit a humidity sensitivity of −288.2 pm/%RH, suitable for respiration monitoring applications (Fig. 4g).[58] Hybridizing graphene with porous frameworks or polymers not only enhances microcavity mechanical stability, but also accelerates sensor response. Furthermore, CNT-based composites integrated into microcavity architectures substantially boost electrical performance, elevating their utility in high-precision sensing platforms. Tou *et al.* develop microporous sensing layers using multi-walled carbon nanotubes (MWCNTs), ether-functionalized surfactants, and PDMS (Fig. 4h),[59] while layered CNT paper structures self-assemble into conductive microcavities that facilitate enzyme cascade electrochemical reactions (Fig. 4i).[60]

Other materials. In addition to conventional material systems, emerging functional materials, such as piezoelectric ceramics and ion gels, are also being actively explored within microcavity-based sensing architectures. Li *et al.* develop an ultrathin wearable device that integrates piezoelectric ceramic (PZT)-5H patches with silicone-encapsulated micro-air cavities, enabling wireless and continuous blood pressure monitoring.[61] Additionally, porous ion gels fabricated *via* microbubble templating exhibit an ultrahigh pressure sensitivity of 684.4 kPa^{-1}, highlighting their promise for next-generation wearable pressure sensing platforms.[62] Compared to inorganic semiconductor devices, photoplethysmography (PPG) sensors based on organic polymer semiconductors enable seamless integration with human tissue and significantly reduce power consumption to 9.96 μW.[63] These functional materials broaden the applicability of microcavity sensors and introduce novel strategies for wireless monitoring, conformal integration, and energy-efficient sensing.

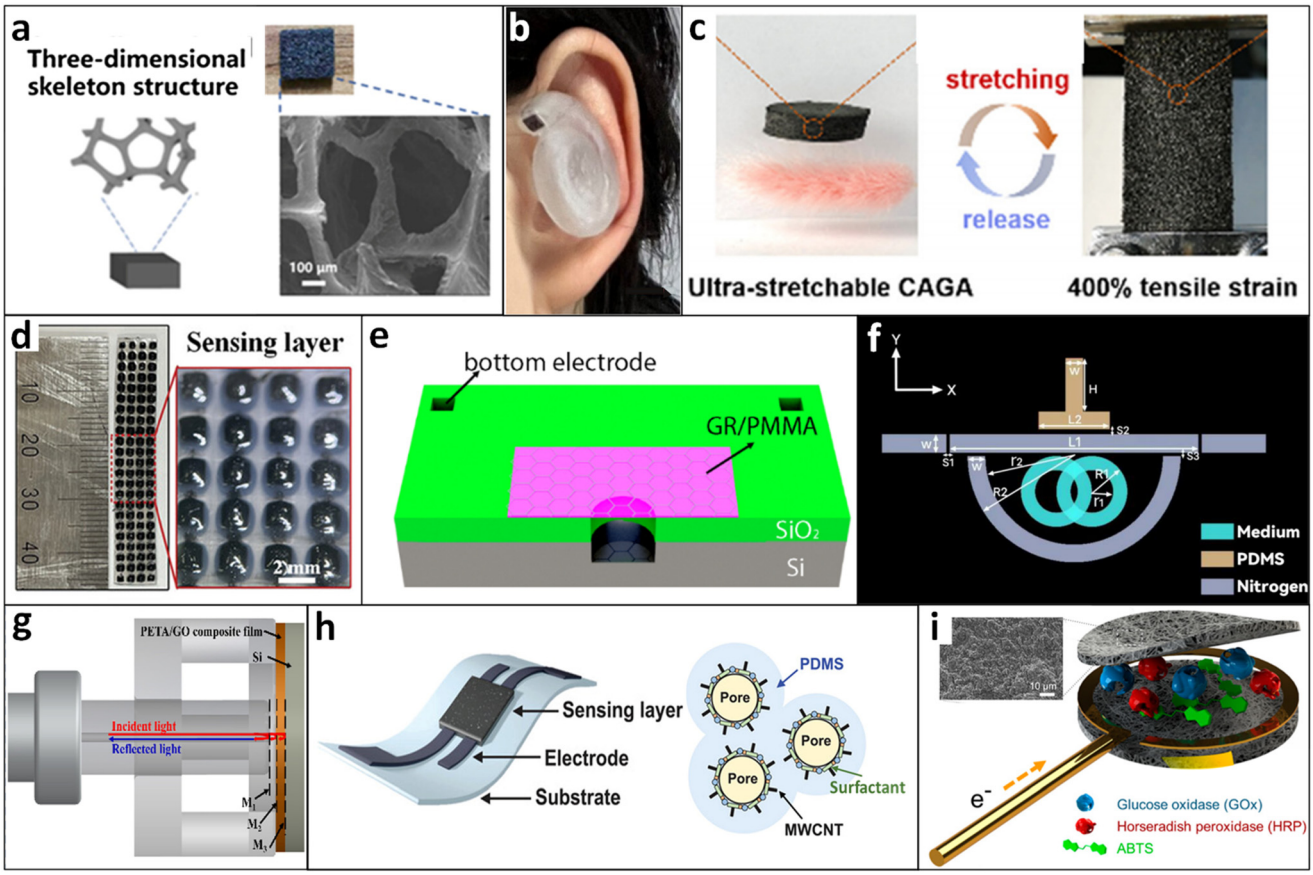

Fig. 4 Various sensors fabricated from carbon-based materials. a. Schematic and SEM images of three-dimensional graphene foam used for constructing thermoacoustic loudspeakers.[51] Reproduced with permission from ref. 51. Copyright (2024) American Chemical Society. b. A photograph of a snail-shaped cavity loudspeaker worn on the human ear. The device is connected to the bottom of the cavity inlet to generate sound waves, and the acoustic signals are amplified and directed toward the ear.[29] Reproduced with permission from ref. 29. Copyright (2025) AAAS. c. Photographs of a graphene aerogel sensor in ultra-stretchable condition and under 400% tensile strain.[54] Reproduced with permission from ref. 54. Copyright (2023) Royal Society of Chemistry. d. An optical microscopy image of a strain-insensitive CNT–PDMS tactile sensing layer. Each sensing unit has a dome-shaped architecture.[55] Reproduced with permission from ref. 55. Copyright (2025) Wiley-VCH GmbH. e. A cross-sectional schematic of a graphene/PMMA closed-cavity ultrasonic sensor. An air gap of 105 μm is formed by the suspended membrane and the silicon substrate.[56] Reproduced with permission from ref. 56. Copyright (2023) MDPI. f. A schematic illustration of a tri-modal sensor unit for refractive index, temperature, and pressure sensing, based on an SNG coupled resonator. The graphene layer is deposited inside the dual-ring and inverted-T resonator structures.[57] Reproduced with permission from ref. 57. Copyright (2024) IEEE. g. A schematic of a PETA/GO composite film optical microcavity sensor.[58] Reproduced with permission from ref. 58. Copyright (2024) American Chemical Society. h. A schematic of a thin-film soft pressure sensor composed of a substrate, electrodes, and sensing layer, along with a diagram showing the micropore network formed within the sensing layer.[59] Reproduced with permission from ref. 59. Copyright (2023) Wiley-VCH GmbH. i. A schematic of a dual-enzyme conductive microcavity, with black regions representing CNT buckypapers. A 3D exploded view illustrates the concept of microcavity.[60] Reproduced with permission from ref. 60. Copyright (2024) MDPI.

Brief summary. The performance limits of microcavity sensors are fundamentally governed by the multidimensional interplay among the electrical conductivity, mechanical compliance, and multiphysical coupling efficiency. With low Young's modulus and ease of processing, flexible polymers are well-suited for fabricating deformable cavities and porous sensing layers; high electrical conductivity and reconfigurability of LMs make sensors with excellent stretchability and self-repairing capacity; carbon-based nanomaterials, due to their exceptional electrical and thermal transport properties, enhance the sensitivity in detecting mechanical, acoustic, and optical signals; emerging functional materials, for example ion gels, also expand the applicability of microcavity-assisted devices. The selection of materials not only affects sensing performance, but also largely determines the design strategies of microcavity structures and the feasibility of functional integration.

Fabrication techniques

Fabrication strategies for microcavity-enabled sensors are transitioning from traditional planar micromachining toward three-dimensional, customizable manufacturing paradigms.

Laser processing method. Laser-induced PI surfaces can yield porous graphene, which, when transferred onto flexible substrates, enables pressure sensitivities up to 15.4 kPa^{-1}.[35] Laser thermal forming, assisted by photothermal absorbers

and porogens, induces controlled bubble formation within PDMS, producing patterned arrays of self-supporting microcavities (Fig. 5a).[44] Laser processing not only precisely fabricates porous architectures on flexible substrates, but also directly prepares microchannels and infuses LM to yield integrated conductive tracks. A CO_2-laser inscribes around 60 μm graphite trenches in LM/PI laminates, which are subsequently capped with PDMS, thus creating a photothermally actuated, strain-sensing conduit.[64] Femtosecond laser direct-writes microgrooves as narrow as 5 μm in Cu/elastomer hybrids, enabling ultra-high-resolution, stretchable sensors.[65] Laser etching of a 200 μm-thick film template followed by LM transfer engenders a 0.3–10 mm adjustable microfluidic network in Ecoflex elastomer.[66] Laser-based techniques allow for high-precision structuring of microcavities, microchannels, and conductive paths on flexible substrates, featuring high resolution, rapid prototyping, and broad material compatibility, making it suitable for constructing multifunctional flexible electronics.

Sacrificial templating method. A range of sacrificial materials, including sugar powder, deionized water, PVA, sodium chloride (NaCl), and other porogens, are employed to template porous microcavities or conductive networks within composite or polymeric matrices *via* hot pressing or solvent dissolution (Fig. 5b).[31,41,43–45] Alternatively, gaseous templates, *via* microbubble generation or self-foaming silicone, facilitate the formation of uniform pore networks, resulting in compressible, elastic microcavity structures.[42,62] This technique employs sacrificial templates to generate well-defined microchannels or cavities within polymer matrices, offering a facile and versatile approach, especially advantageous for fabricating porous architectures and conductive networks.

3D printing techniques. Qiu *et al.* modify the rheological properties of LM by incorporating SiO_2 nanoparticles, thereby tuning its elastic and viscous moduli, as well as overall viscosity. This approach enables the rapid 3D printing of soft electronic devices based on the modified LM composites.[50] Liu *et al.* employ an indirect 3D printing strategy to construct flexible microchannels. Specifically, acrylonitrile butadiene styrene (ABS) is printed into intricate sacrificial molds, which are then embedded in Ecoflex prepolymer. Upon curing, acetone dissolves the ABS structures, yielding millimetre-scale

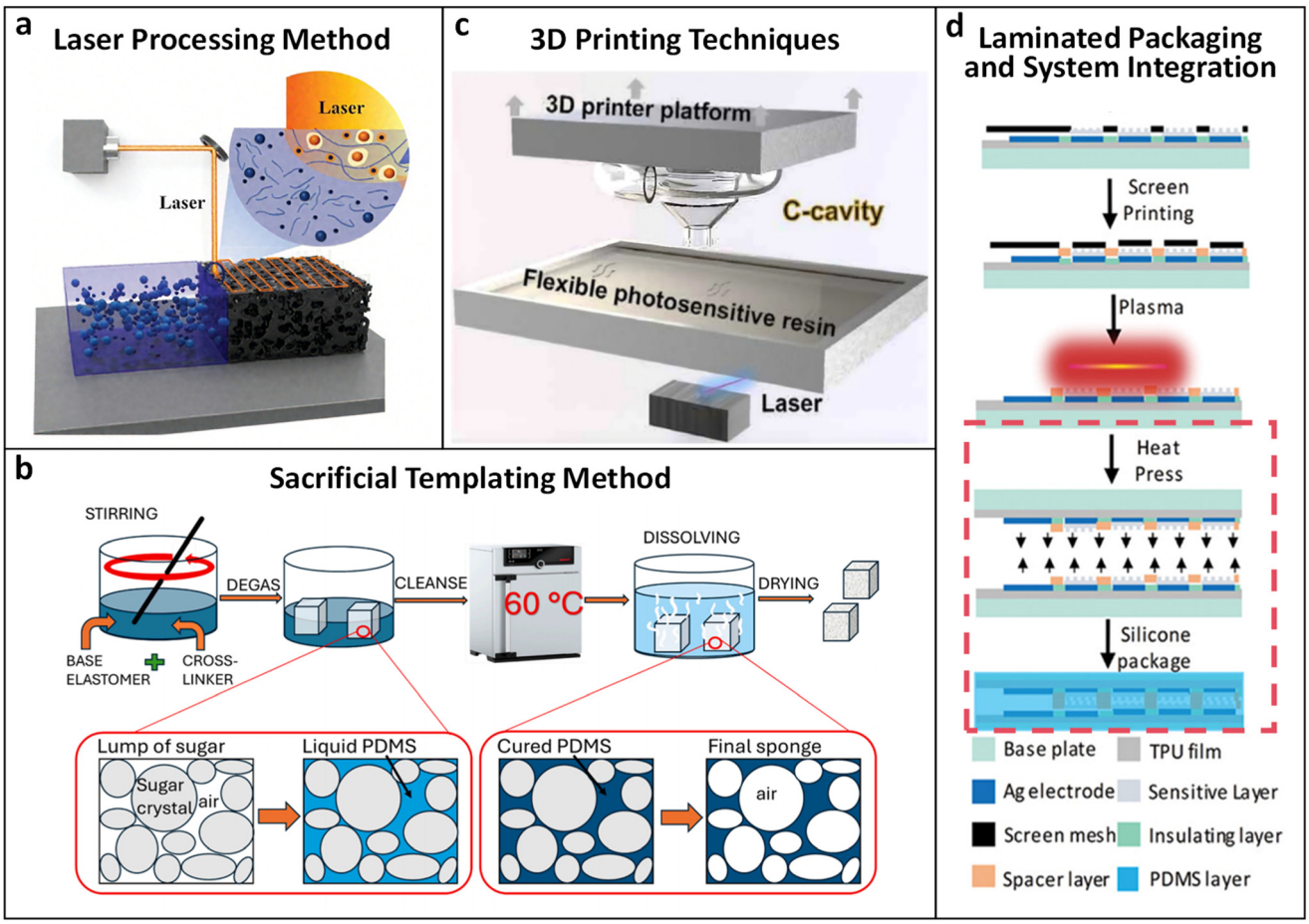

Fig. 5 Fabrication techniques for microcavity-assisted physical sensors. a. Laser processing method. Reproduced with permission from ref. 44. Copyright (2023) Wiley-VCH GmbH. b. Sacrificial templating method. Reproduced with permission from ref. 41. Copyright (2025) Elsevier. c. 3D printing techniques. Reproduced with permission from ref. 29. Copyright (2025) AAAS. d. Laminated packaging and system integration. Reproduced with permission from ref. 27. Copyright (2025) Wiley-VCH GmbH.

3D conductive microchannels.[67] Wei *et al.* utilize photocurable resin-based 3D printing to rapidly fabricate conch-shaped resonant cavities (Fig. 5c).[29] 3D printing offers flexible design freedom for microcavity structures, enabling the rapid and customizable fabrication of complex prototypes, and represents a pivotal technology for advancing personalized microfluidic sensors.

Laminated packaging and system integration. Multilayer lamination and vacuum encapsulation facilitate the integration of PZT elements, PDMS-based microcavities, and hybrid flexible–rigid circuits into a 4 mm-thick, continuously monitoring wearable blood pressure patch.[61] Wang *et al.* bond pre-assembled layered structures using vacuum-assisted thermal lamination, followed by hot pressing to finalize the encapsulated flexible pressure sensor array (Fig. 5d).[27] Lamination-based encapsulation employs multilayer assembly and thermal compression techniques to integrate microcavities, sensing layers, and electronics, facilitating sensor miniaturization, functional integration, and output stability.

Brief summary. In summary, from laser processing and sacrificial templating to 3D printing and laminated packaging, diverse fabrication strategies enable precise construction of microcavity structures with tunable geometry and integrated functionality. These methods collectively support scalable, customizable, and high-performance sensor manufacturing.

Microcavity-assisted physical sensors exhibit diversity in both materials and fabrication techniques. Researchers design sensors and microcavities based on application scenarios. By reasonably selecting and combining different materials, such as polymers, LMs, carbon-based materials, and other special materials, it is possible to achieve higher sensitivity, faster response, and improved stability in microcavity designs. Simultaneously, the synergy of advanced fabrication techniques enables precise control over cavity geometry, pore size distribution, and wall surface functionalization across micron to millimeter scales. These microstructures are further integrated with self-powered mechanisms, signal conditioning modules, and artificial intelligence (AI)-driven algorithms, collectively establishing a robust foundation for the development of next-generation, high-sensitivity, multi-parametric, and large-area manufacturable microfluidic physical sensors.

Sensing principle, structure, and application of microcavity-assisted sensors

Building upon these advanced processes and materials, researchers have developed various microfluidic sensors for physical signal detection. Practical applications reveal that different materials exhibit distinct compatibility preferences in sensor architecture and operational principles, due to their inherent differences in electrical, mechanical, and thermal properties. For instance, elastic polymers are commonly used to construct flexible resistive and capacitive sensors owing to their excellent compressibility and dielectric characteristics. LMs demonstrate high conductivity and flow reconfigurability, making them widely applicable in resistive microchannel structures. Ultra-thin graphene's superior electrical and thermal conductivity plays a pivotal role in acoustic resonance and thermoacoustic transduction sensing. To clarify the coupling pathways between material systems and sensor architectures, Table 1 systematically outlines commonly used material systems for microcavity-assisted physical sensors, summarizing the applicability and functional emphases of mainstream material systems in microcavity construction. These materials support diverse sensing mechanisms, including resistive, capacitive, triboelectric, acoustic, and optical/thermal sensing. Researchers typically need to select optimal structural configurations and sensing mechanisms based on practical application requirements.

Mechanical sensing

Resistive sensing

Pressurizable microcavities based on sealed airbag architectures. Within flexible resistive-type sensors, sealed airbag structures represent a canonical microcavity configuration, characterized by high tunability, large strain adaptability, and strong engineering controllability. These properties make them especially well-suited for the development of active pressure-regulated sensing systems. By employing inflatable or pre-pressurized cavities, such structures generate predictable stress responses under external mechanical loading or active pneumatic input, facilitating improved sensor-skin conformity, enhanced detection of subtle signals, and the seamless integration of multimodal sensing and physiological monitoring functionalities.

Luo *et al.* integrate a PDMS-based spherical sealed microcavity with a laser-induced graphene (LIG) conductive layer to develop a high-performance flexible resistive sensor tailored for non-invasive, single-vessel blood pressure monitoring (Fig. 6a).[35] The encapsulated air cavity functions as a mechanical buffer, significantly enhancing the electromechanical transduction efficiency while mitigating fatigue-induced degradation of the LIG conductive network under sustained or high-intensity loading. When coupled with a dual-stage convolutional neural network, the system achieves clinically relevant accuracy, with a diastolic pressure error of less than 0.5 mmHg and a systolic pressure error of less than 2.1 mmHg, in estimating blood pressure from a single vessel, thus offering a cost-effective and non-invasive approach to wearable hemodynamic monitoring.

Beyond blood pressure monitoring, actively pressurized sensing mechanisms have also been widely applied in pulse diagnostics. Drawing inspiration from traditional Chinese medicine (TCM) palpation techniques, Wang *et al.* develop a fully printed, flexible sensor array that integrates an airbag-based microcavity array for simultaneous acquisition of pulse signals at the "Cun", "Guan", and "Chi" positions (Fig. 6b).[27] The microcavity structure supports multi-phase active

Table 1 Coupling pathways between material systems, sensing mechanisms, and application scenarios in microcavity-assisted sensors

Material categories	Specific materials		Features	Selected properties	Preferred sensing mechanism	Typical application scenarios
Polymer	Elastomer	PDMS, Ecoflex	High elasticity, low young's modulus, large deformability	Young's modulus (E): 100–2000 kPa;[68] relative permittivity (ε_R): 2.6–2.8 (ref. 69 and 70)	Resistive, capacitive, triboelectric, acoustic, and photothermal	Compressible microcavities, multimodal sensing, electronic skin, health monitoring, and wearable motion tracking
		PU	With balanced strength and flexibility, good thermal stability	Young's modulus (E): 1–200 MPa;[71] thermal degradation temperature: >300°C (ref. 72)		
	Engineering plastic	PI	With good mechanical strength, thermal stability, and strong film-forming properties	Young's modulus (E): 5.89 GPa;[73] relative permittivity (ε_R): 2.1–2.94;[74] glass transition temperature (T_g): >350°C (ref. 75)	Capacitive (electret-based), resistive	Microcavity-assisted capacitive sensor substrate, flexible circuit support, laser-micromachined encapsulation
		PET		Young's modulus (E): 1.07 GPa;[76] relative permittivity (ε_R): 3.1;[77] glass transition temperature (T_g): 80°C (ref. 77)		
	Hydrophilic polymer	PVA	Water-soluble, highly biocompatible	Young's modulus (E): 0.04–7 GPa (ref. 78)	Resistive	Flexible biosensing layer, capacitive/ion-conductive dielectric, skin/physiological signal acquisition
	Fluorinated polymer	PVDF	Chemically stable, hydrophobic, some with piezoelectric or charge-holding characteristics	Piezoelectric coefficient (d_{33}): 13–28 pC/N, relative permittivity (ε_R): 12 (ref. 79)	TENG-based piezoelectric electret sensing	Non-contact touch sensing, motion/posture recognition, remote interaction, humidity monitoring
		PTFE/PFA composite film		Piezoelectric coefficient (d_{33}): 23.8 pC/N (ref. 36)		
LM	EGaIn: gallium–indium alloy (75.5% Ga, 24.5% in)		Liquid at ambient conditions, excellent electrical conductivity, mechanical deformability, and strong compatibility with soft elastomers	Electrical conductivity (σ): 3.4×10^6 S m^{-1}, melting point (T_m): 15.7 °C (ref. 80)	Resistive (microchannel strain-based)	3D pressure mapping, strain sensing, bioelectrical monitoring, wearable e-skin
	Galinstan: gallium–indium–tin alloy (68% Ga, 21.5% in, 10.5% Sn)			Electrical conductivity (σ): 3.8×10^6 S m^{-1}, melting point (T_m): −19 °C (ref. 80)		
Carbon-based material	Graphene		Excellent electrical and thermal conductivity, two-dimensional structure	Thermal conductivity (κ): 5300 W m^{-1} K^{-1}, electron mobility (μ): 3.5×10^5 cm^2 V^{-1} s^{-1}, SSA: 2630 m^2 g^{-1} (ref. 81)	Acoustic, thermoacoustic, resistive, triboelectric, optical	Thermoacoustic speaker, acoustic sensing, micro-pressure detection
	CNT		One-dimensional flexible conductor combining conductivity and mechanical flexibility	Thermal conductivity (κ): 3500 W m^{-1} K^{-1};[82] electron mobility (μ): 2800–5400 cm^2 V^{-1} s^{-1};[83] SSA: 1315 m^2 g^{-1} (ref. 84)	Resistive, triboelectric, thermal	Strain sensing, conductive film
Other functional materials	PZT		High piezoelectric response, strong electromechanical coupling, and consistent response	Piezoelectric coefficient (d_{33}): 750 pC/N (ref. 85)	Triboelectric, capacitive, photothermal	Passive sensing, non-contact interaction, flexible HMI
	Hydrogel		Hydrophilic and flexible, with ionic conductivity and excellent biocompatibility	Water content: 70–90 wt%;[86] ionic conductivity: 10^{-5}–30 S cm^{-1} (ref. 87)	Capacitive sensing (flexible electrolyte-based), electrochemical sensing	Skin-interface sensing, physiological signal detection, flexible iontronic devices

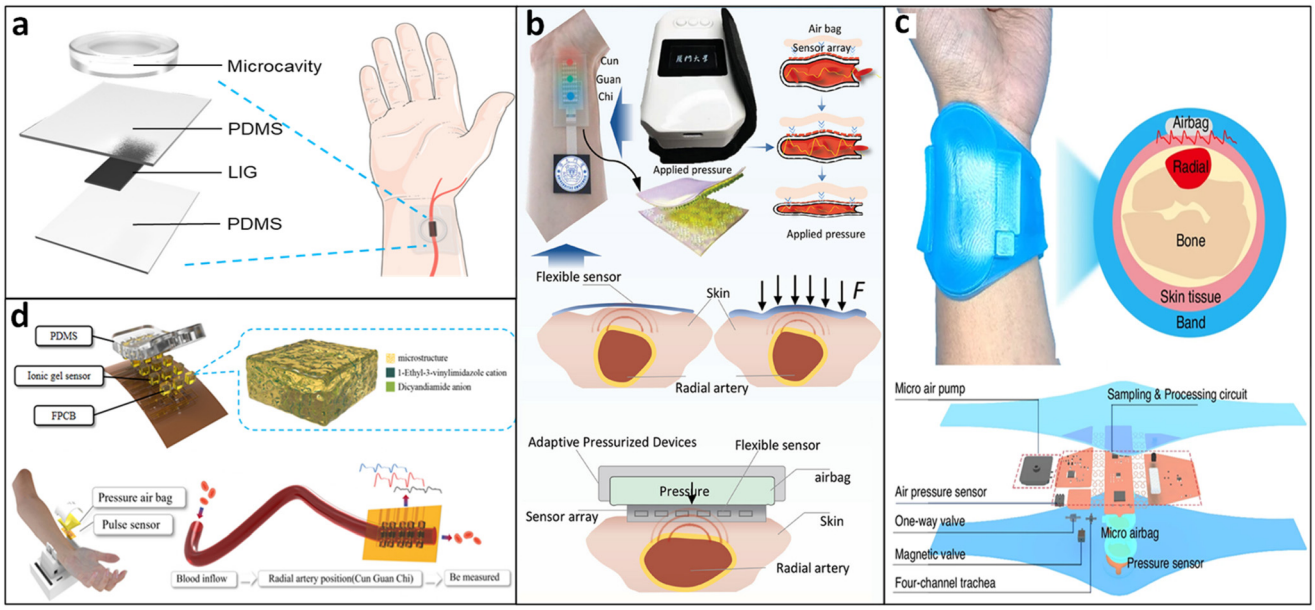

Fig. 6 Closed airbag-assisted microcavity-based sensing systems. a. A flexible resistive pressure sensor composed of a spherical PDMS microcavity and a laser-induced graphene layer, enabling noninvasive single-vessel blood pressure monitoring.[35] Reproduced with permission from ref. 35. Copyright (2024) Springer Nature. b. A fully printed flexible sensor array with integrated airbag microcavities for simultaneous pulse monitoring at three radial artery positions *via* multi-stage active pressurization.[27] Reproduced with permission from ref. 27. Copyright (2025) Wiley-VCH Verlag GmbH & Co. KGaA, Weinheim. c. A multi-channel wearable sensing platform combining silicone airbags and ionic conductive films for synchronized pulse acquisition and real-time blood pressure estimation.[33] Reproduced with permission from ref. 33. Copyright (2024) Springer Nature. d. A 3D pulse sensing array with multiple airbags and machine learning-assisted signal processing for atrial fibrillation classification.[88] Reproduced with permission from ref. 88. Copyright (2025) American Chemical Society.

pressurization, effectively emulating the dynamic "palpation" process to enhance the conformal interface between the skin and sensor surface, while modulating the sensing depth to capture pulse waveforms at varying vascular layers. The system exhibits consistent performance across diverse participants, body postures, and activity states, demonstrating the microcavity's engineering adaptability under complex pressure modulation conditions.

Based on the concept of pulse diagnosis, Zhao *et al.* introduce a multi-channel, actively pressurized flexible pulse monitoring platform, integrating silicone-based airbag cavities with flexible ion-conductive membrane arrays to enable synchronized pressure measurements at three distinct diagnostic points (Fig. 6c).[33] Coupled with a neural network model based on nine static pressure segments and pulse wave amplitude, the platform provides real-time predictions of systolic and diastolic blood pressures.

In addition, Cao *et al.* expand the multi-airbag structure to a three-dimensional, dynamically controlled pulse array platform, incorporating a machine learning model to develop an atrial fibrillation classification system, thereby achieving the digitalization of traditional pulse diagnosis data (Fig. 6d).[88] This platform integrates active pressurization, adaptive deformation, and AI-assisted diagnostic capabilities, marking a paradigm shift in microcavity-based health sensing systems from simulation-based sensing to cognitive diagnostic applications.

The sealed airbag microcavity structure modulates the sensor state through active deformation control, thereby enhancing both the sensitivity and reliability of flexible resistive sensors, while offering a systematic design pathway for the high-precision acquisition of complex physiological signals. The structure's tunability, coupled with its continuous and controllable signal response, positions it as one of the most prominent application paradigms in contemporary microcavity-assisted flexible microfluidic sensing technologies.

Microchannel structure with LM infusion. Beyond the actively pressurized microcavity design based on sealed airbag structures, another prevalent microcavity configuration employed in resistive flexible sensors is the LM microchannel structure. Microchannels, fundamentally characterized as deformable microcavities with confined space, typically form dynamic conductive pathways through the injection of LM. This structure, while preserving the flexibility and wearability of the device, enables substantial resistance changes in response to variations in the cross-sectional pressure of the channel, thus offering exceptional sensitivity and structural stability. The fundamental equation governing the relationship between resistance change and stress variation in LM microchannels is as follows:

$$\Delta R = R - R_0 = \rho L\left(\frac{1+\varepsilon}{(w+\Delta w)(h+\Delta h)} - \frac{1}{wh}\right) \quad (1)$$

In eqn (1), R and R_0 denote the resistance of the microchannel under stretched and unstretched conditions, respectively. ρ represents the resistivity of the LM, L is the length of the microchannel, while w and h are the width and height of

the microchannel, respectively. Δw and Δh refer to the variations in the microchannel's width and height during stretching, and ε is the applied strain. The sensitivity of the sensor is generally characterized by the gain factor (GF), as defined by eqn (2):

$$GF = \frac{\Delta R/R_0}{\varepsilon} \quad (2)$$

GF is employed to quantify the resistance change of the LM microchannel sensor under unit strain. A higher GF value indicates a more robust stress response capability, which is generally achieved by optimizing the channel's geometric structure.

In the field of resistive sensing, utilizing LM-filled microchannels to fabricate high-sensitivity pressure sensors is a widely adopted technique. Wu *et al.* introduce an innovative structural design in which convex microarrays (CMs) are embedded within the LM channel (Fig. 7a).[89] By integrating convex structures into the PDMS microchannel, the degree of deformation in the channel's cross-section during pressurization is effectively enhanced, leading to increased sensitivity to 4.3×10^{-2} kPa^{-1}, while maintaining a measurement range of up to 340 kPa. The device has been successfully applied in pulse detection, finger bending, gait analysis, and gesture recognition scenarios.

Gul *et al.* develop a soft sensor using LM with a dome-shaped design, which, when combined with AI algorithms, leads to the development of a flexible sensor system capable of three-dimensional stress differentiation (Fig. 7b).[90] The modular LM channel structure can resolve loading discrepancies in the *X*, *Y*, and *Z* directions. By incorporating machine learning models, this system achieves advanced posture and motion recognition, offering innovative perspectives for flexible robotics and multimodal HMI.

Subsequently, Luo *et al.* employ geometrically tunable structures to optimize the deformation response of microchannels and introduce Peano fractal microchannels (Fig. 7c).[15] The Peano fractal not only increases the strain sensing density per unit area, but also through the optimization of structural geometry, delays the fracture point of the LM's conductive path, thus expanding the effective detection range. Their study highlights the importance of embedded structures in regulating conductive pathways within microchannels and demonstrates that engineering the geometry of

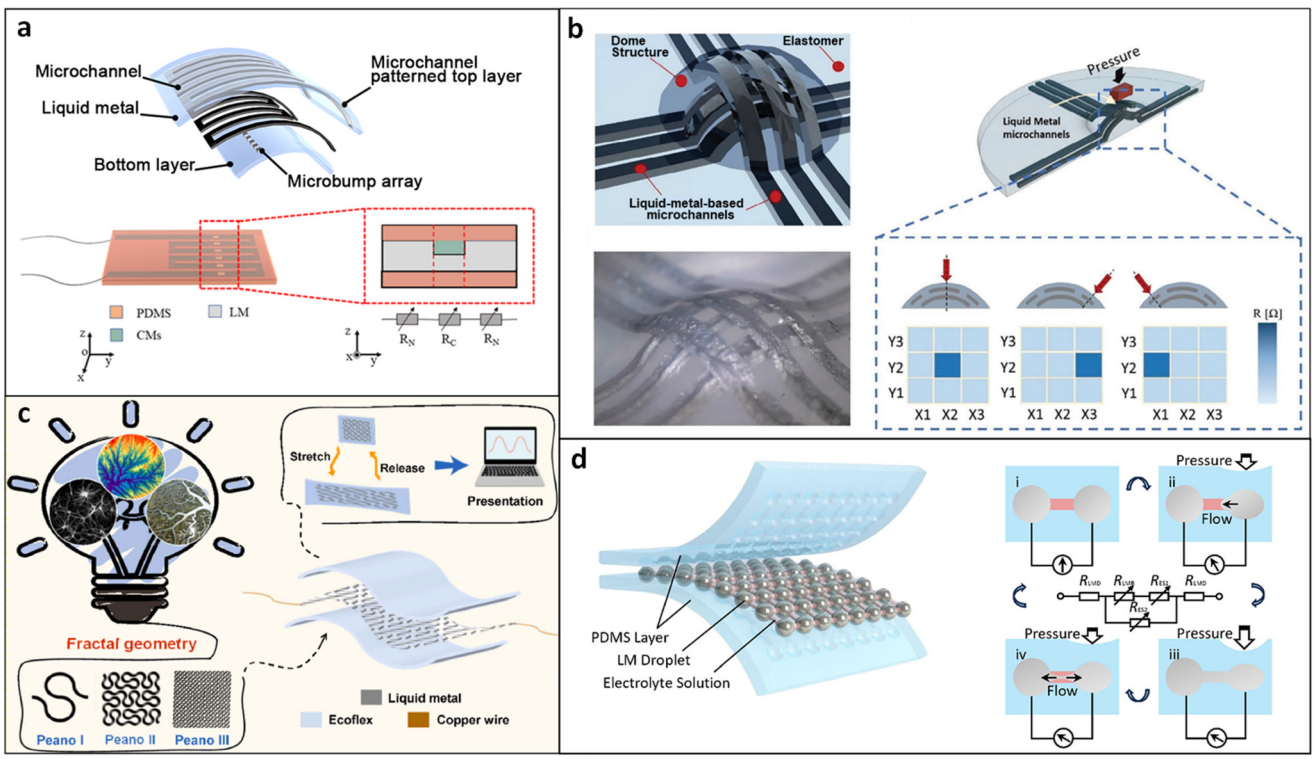

Fig. 7 Microchannel-based resistive sensors with LM. a. A soft resistive sensor integrating CMs within a PDMS-LM microchannel to enhance cross-sectional deformation and improve sensitivity, applied in pulse monitoring, gait analysis, and gesture recognition.[89] Reproduced with permission from ref. 89. Copyright (2023) IEEE. b. A dome-shaped microchannel sensor that differentiates multi-axis pressure distribution (*X*, *Y*, *Z*) and supports intelligent stress recognition through machine learning models.[90] Reproduced with permission from ref. 90. Copyright (2024) Wiley-VCH Verlag GmbH & Co. KGaA, Weinheim. c. A Peano-type fractal microchannel structure that enhances stretchability and sensing density by optimizing the conductive path geometry of the LM.[15] Reproduced with permission from ref. 15. Copyright (2023) Springer Nature. d. A pressure-sensitive structure based on the reversible contact behavior of LMDs, enabling dynamic resistance switching for applications such as physiological signal imaging and throat motion monitoring.[30] Reproduced with permission from ref. 30. Copyright (2025) Wiley-VCH Verlag GmbH & Co. KGaA, Weinheim.

microcavities can achieve a synergistic optimization of sensitivity, stretchability, and stability.

Building on this, Dong *et al.* introduce a novel pressure sensing structure based on the reversible contact behavior of liquid metal droplets (LMDs). By precisely controlling the microchannel geometry and electrolyte filling, they achieve controllable contact and disconnection of LMDs under varying pressures, leading to stable resistance changes and enabling "switch-like" dynamic resistance regulation (Fig. 7d).[30] It has been successfully applied to complex physiological signal sensing scenarios, including two-dimensional image reconstruction and pharyngeal motion detection.

Brief summary. In summary, LM microchannels, as dynamic closed microcavity structures, exhibit good tunable performance in flexible pressure sensor design. Different studies have enhanced critical metrics, such as high sensitivity, broad dynamic range, and multimodal responses through strategies like the incorporation of microstructure arrays, directional recognition channel designs, and LMD reversible contact. These advancements highlight the vast potential of LM microcavity structures in wearable health monitoring and integrated smart systems.

Recent research has introduced the use of micro-cage structures to achieve local regulation of microscopic strain, representing an innovative microcavity configuration. This structure has demonstrated significant advantages in enhancing the resolution and anti-crosstalk capabilities of array sensors, making it highly suitable for multi-pixel pressure sensing systems. Zhang *et al.* implement micro-cage strain-constrained structures in PDMS using a photo-crosslinking strategy.[91] By employing ultraviolet-induced crosslinking inhibition, they introduce locally uncrosslinked regions in the PDMS, thereby forming microcavity units with localized strain characteristics that effectively constrain deformation diffusion within each pixel. The micro-cage structure reduces mechanical crosstalk between array elements by 90.3%, while maintaining an excellent sensitivity of 18.94 kPa^{-1}. Additionally, it achieves a spatial resolution exceeding 4000 ppi and a minimum perceptible weight of 1 g (Fig. 8). This approach offers an effective structural solution for high-density and low-crosstalk flexible array sensors.

Capacitive sensing

Porous dielectric layer. To design flexible capacitive tactile sensors, the structure and dielectric properties of the dielectric layer are critical to the overall sensing performance.

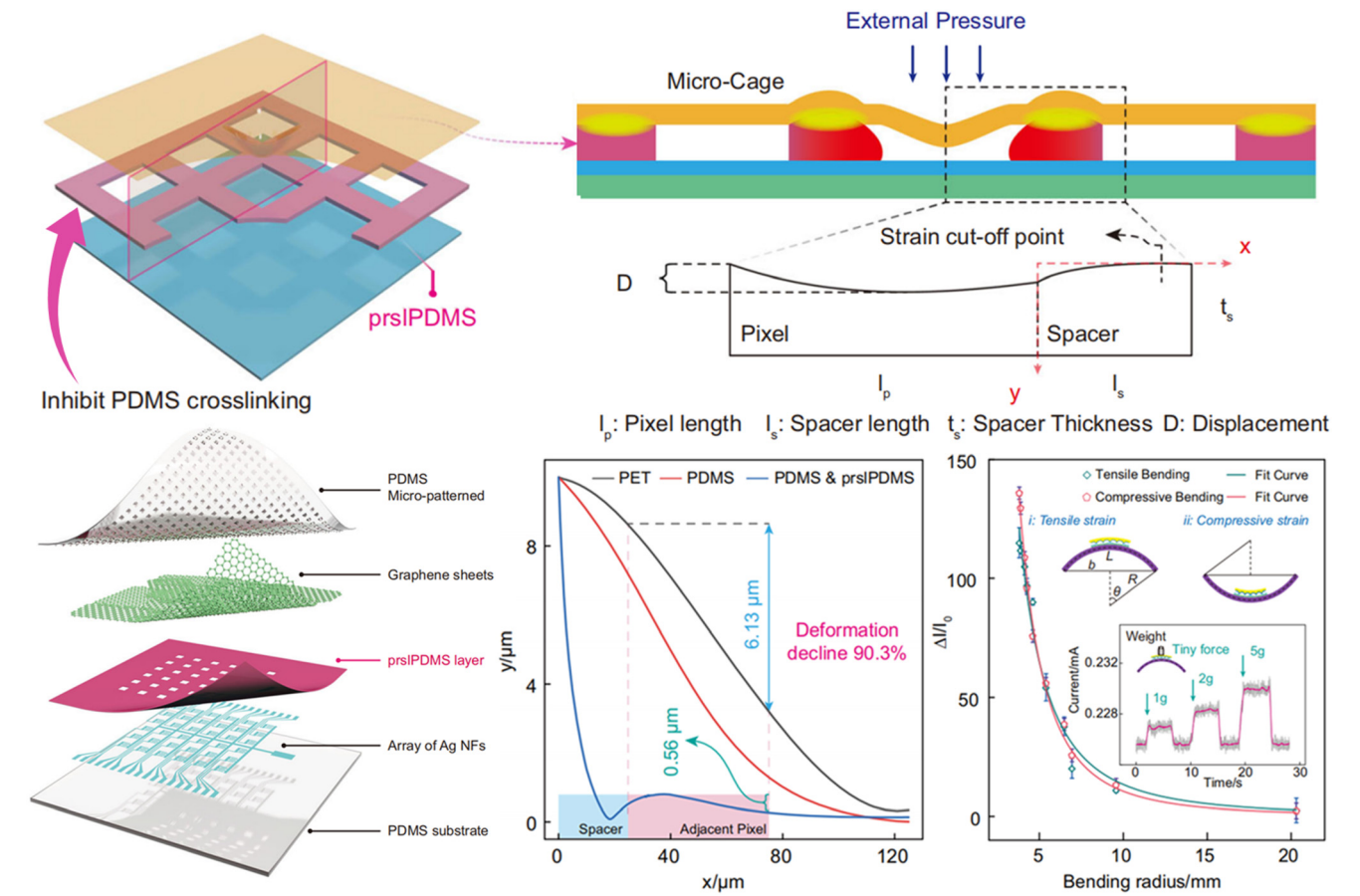

Fig. 8 Micro-cage structured stretchable pressure sensor array and its key performance metrics.[91] A photo-crosslinking strategy is used to create localized uncrosslinked regions in PDMS, forming micro-cage units that confine strain within individual pixels, reduce crosstalk by 90.3%, and achieve a minimum detectable weight of 1 g. Reproduced with permission from ref. 91. Copyright (2023) Springer Nature.

Traditional homogeneous dielectric materials face limitations in terms of compressibility, dielectric constant tunability, and response speed, making it challenging to achieve both high sensitivity and wide range response. In contrast, porous materials, filled with numerous micro-scale cavities, naturally form a three-dimensional microcavity network. By introducing micro-scale air cavities within the dielectric, porous dielectric layers not only reduce the overall dielectric constant, but also enhance compressibility under applied forces, thus improving capacitive response sensitivity and signal-to-noise ratio. This structural design has significant potential for integration into flexible electronic skin systems, particularly for tactile and non-tactile integrated sensing, and demonstrates excellent performance in both static pressure monitoring and dynamic interface interactions.

Based on the aforementioned design principles, Wang *et al.* develop a dual-modal flexible electronic skin, utilizing digital light processing 3D printing to construct micro-spike electrode structures, and introducing a porous PDMS dielectric layer *via* a sacrificial template method to create microstructure–microcavity composite capacitive sensing units (Fig. 9a).[28] The porous structure not only reduces the dielectric constant, but also enhances compressive deformation response, resulting in a high sensitivity of 1.672 kPa^{-1} within a pressure range of 0–20 kPa, with mass detection capability down to 1 g and non-contact recognition ability up to 10 cm. Under a similar structural framework, Wu *et al.* further propose a flexible sensing array integrating porous dielectric layers, micro-spike electrodes, and edge electric field sensing mechanisms (Fig. 9b). The porous sponge structure, made of PDMS with hundreds of micron-sized holes, is filled with ionic liquid and sandwiched between two layers of flexible conductive fabric, forming a highly sensitive variable capacitance structure. Non-contact recognition is enabled by the edge electric field interference mechanism, and dynamic gesture and 3D morphology sensing with >99% accuracy is achieved through machine learning.[37]

The micron-scale cavities within the porous dielectric layer are crucial in enhancing the compressive response of the device and its sensitivity to edge electric field disturbances. Additionally, they significantly reduce the overall mass, facilitating the maintenance of the device's flexibility and conformability. This microcavity structure, which integrates both performance and lightweight characteristics, serves as a fundamental structural basis for the development of multimodal flexible sensors.

Electret thin film. The electret thin film is a key microcavity material for enabling high-sensitivity non-contact capacitive sensing. It stores permanent charges within, and by constructing a membrane-cavity-electrode microbubble structure, it generates a stable electric field response. This structure offers several advantages, including self-powering, flexibility, and low power consumption, making it particularly suitable for long-range non-contact HMI applications. In such a structure, the

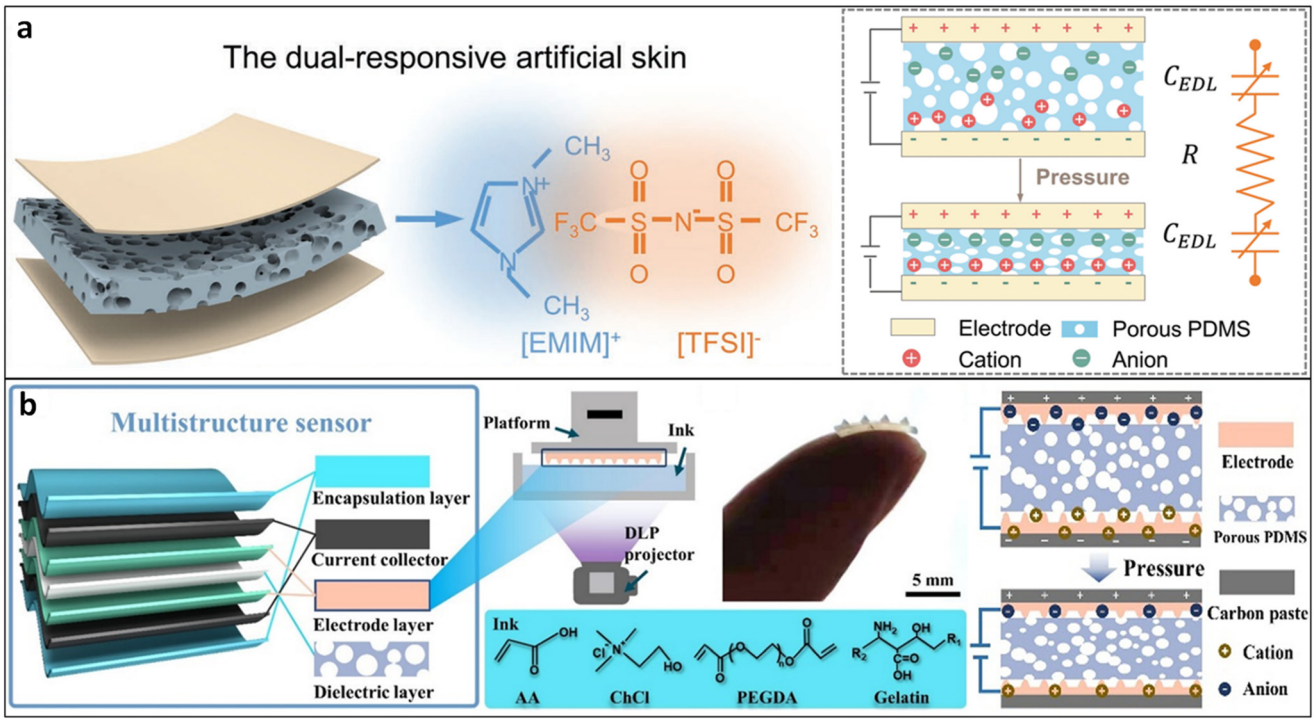

Fig. 9 Porous dielectric layer-based capacitive sensors. a. A dual-responsive electronic skin fabricated *via* DLP 3D printing, integrating microspike electrodes and a porous PDMS dielectric layer to form microstructure–microcavity composite capacitive units.[28] Reproduced with permission from ref. 28. Copyright (2023) Wiley-VCH Verlag GmbH & Co. KGaA, Weinheim. b. A bimodal sensing array composed of ionic liquid-filled porous PDMS and flexible fabric electrodes, enabling edge electric field modulation for touchless and dynamic pressure sensing with >99% gesture recognition accuracy.[37] Reproduced with permission from ref. 37. Copyright (2024) American Chemical Society.

microcavity not only provides dielectric isolation, but also serves as an air gap for stable capacitive response, significantly enhancing sensitivity and signal-to-noise ratio.

Liu *et al.* develop a self-powered flexible non-contact sensor (Fig. 10a), where a fluorinated ethylene propylene (FEP) film and PET substrate composite form a cavity structure. By utilizing corona charging, stable potential and capacitive responses are generated, enabling precise sensing of distances as small as 2 mm. The sensor successfully detects eyelid movements and exhibits a certain degree of resolution for various gestures and spatial positions, showing considerable application potential in the fields of soft robotics and wearable sensing technologies.[92]

Dai *et al.* introduce a flexible electret sensing platform integrated with a variable-spacing electrode array. By utilizing a microcavity structure to adjust the equivalent capacitance response curve with respect to distance, they achieve an ultra-wide sensing range (2–180 mm) and multi-angle 3D recognition capabilities (Fig. 10b).[39] The device enables non-contact multi-point tracking, object posture recognition, and remote sliding gesture interaction through the coupling of electric field disturbances and structural microcavity variations.

In an extended approach, Xu *et al.* integrate electret microcavity structures with optical ranging and acoustic feedback functionalities, constructing an intelligent scanner based on an FEP–air–PET sandwich structure. This system enables 3D spatial depth perception and real-time voice feedback within a self-driven HMI system (Fig. 10c).[32] The device, without any external power input, utilizes structural vibrations to drive a sound wave emitter and adjust the laser scanning angle, allowing for long-range positioning and navigation up to 250 cm. This serves as a representative example of the application of electret microcavity structures in multimodal interaction.

In a non-contact sensing, the electret structure generates an electric field disturbance, whereas in a contact scenario, it induces a charge coupling response. As a result, when applied to contact-based mechanical sensing environments, the signal output transitions to a triboelectric response.

Triboelectric sensing

Triboelectric sensing relies on the surface charge transfer during the contact-separation process of materials, enabling passive, highly sensitive flexible pressure sensing. When integrated with electret or porous microcavity structures, it enhances the device's output stability, response linearity, and spatial adaptability.

Wu *et al.* develop a flexible, self-powered electret pressure sensor array based on a multilayer structure of e-PTFE, PFA, and FEP, with the core being a composite film featuring a

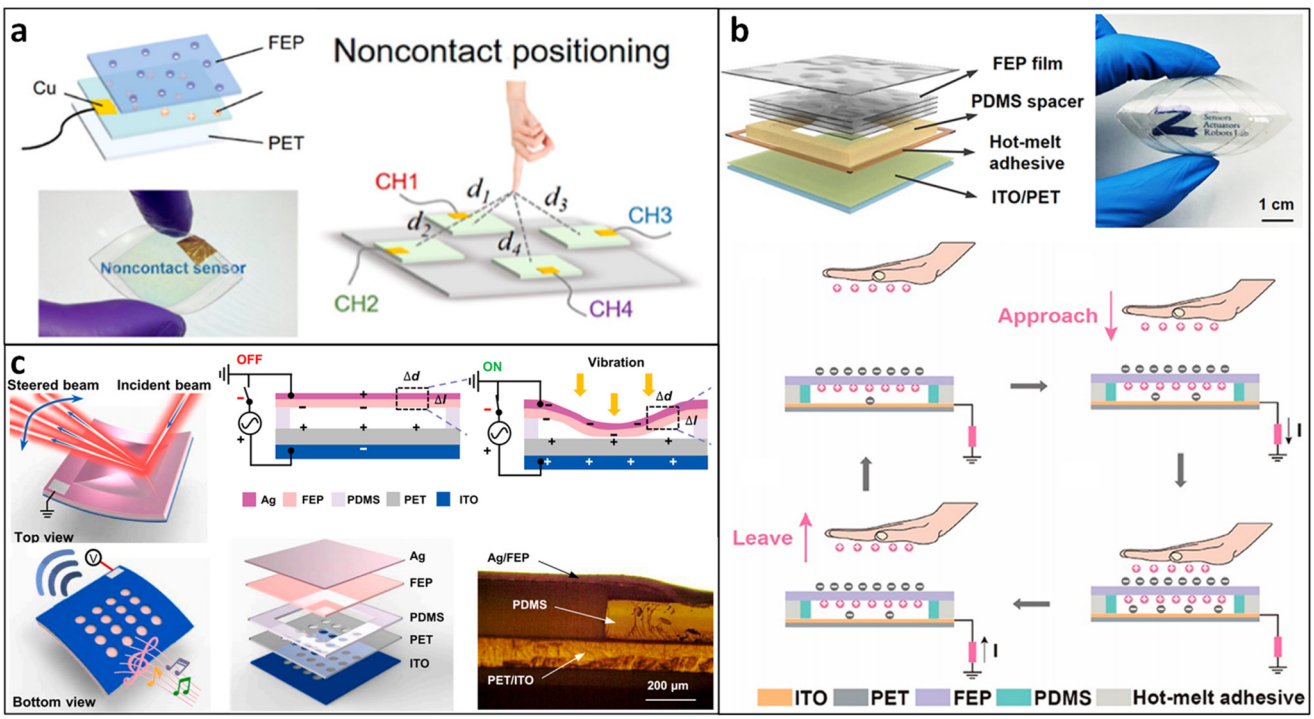

Fig. 10 Electret-based capacitive sensors with non-contact sensing capability. a. A self-powered soft sensor combining FEP film and PET substrate *via* corona charging to form an electret cavity, enabling sub-millimeter distance resolution and gesture recognition for non-contact positioning.[92] Reproduced with permission from ref. 92. Copyright (2024) American Chemical Society. b. A flexible electret sensor platform using a multilayer microcavity structure and variable-spacing electrode array to achieve ultra-wide sensing range (2–180 mm) and 3D posture recognition.[39] Reproduced with permission from ref. 39. Copyright (2023) American Chemical Society. c. An electret actuator integrating optical ranging and acoustic feedback, based on an FEP–air–PET sandwich microcavity that supports multimodal long-range HMI with scanning and voice response functions.[32] Reproduced with permission from ref. 32. Copyright (2024) Elsevier.

microcavity structure (Fig. 11a).[36] The microcavity structure significantly reduces the Young's modulus of the film layer while enhancing sensing performance, achieving a sensitivity of 9 mV N^{-1} over a range of 1.4–13.6 N. The sensor demonstrates excellent performance in real-time monitoring across various human body scenarios (*e.g.*, sound, pulse, and finger joint activities) and during pig knee joint replacement surgery.

Zhou *et al.* develop a respiration-driven self-powered PVDF/cellulose acetate (CA) nanofiber filter material, incorporating a porous fiber network created by electrospinning and an annular cavity composed of copper foil, electrode sheets, and elastic supports (Fig. 11b).[93] This microcavity structure aids in maintaining a stable airflow channel and electric field gradient, thereby enhancing the electrostatic adhesion capacity generated by the triboelectric effect. It exhibits sustained

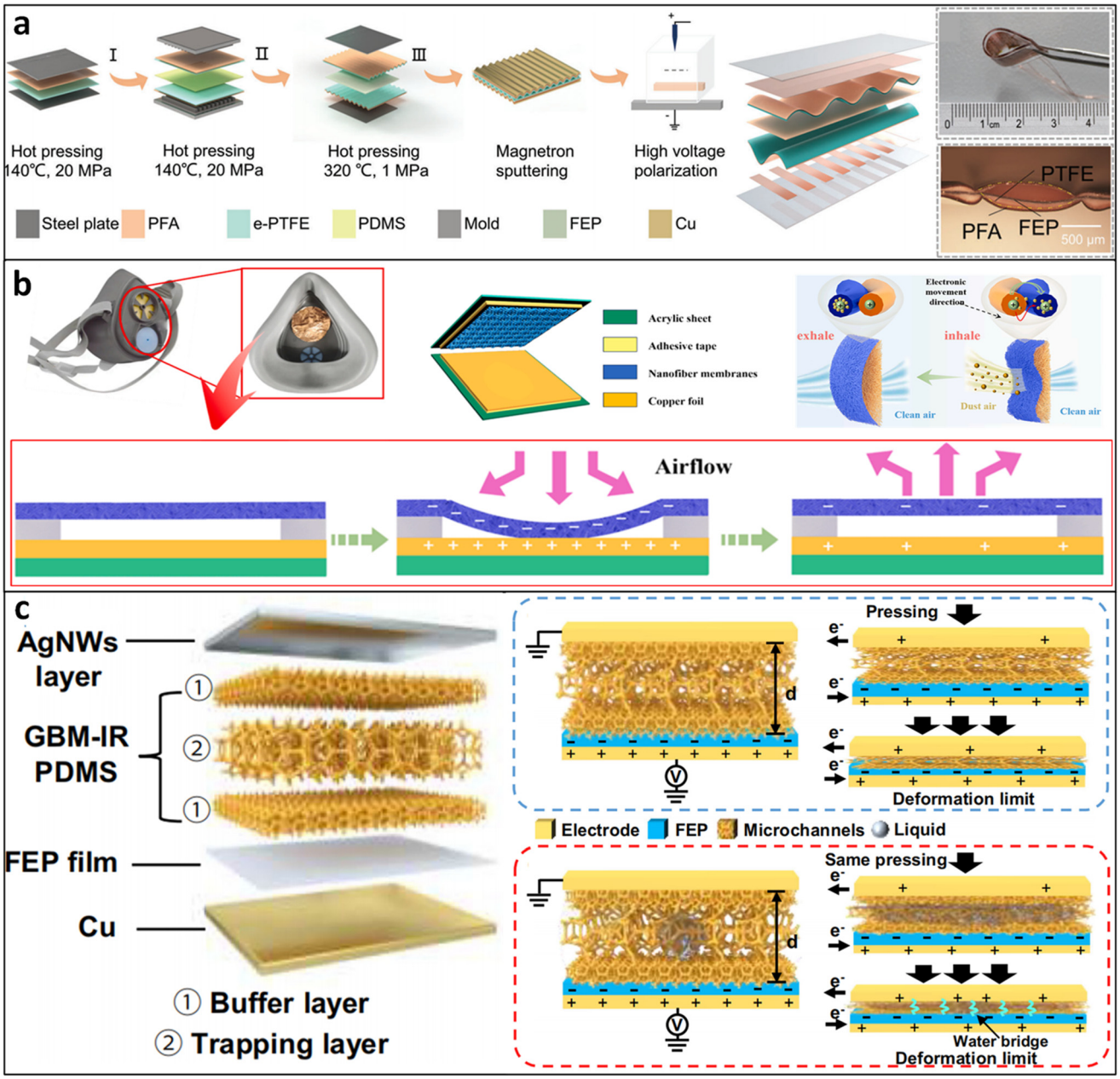

Fig. 11 Triboelectric microcavity-based self-powered sensors. a. A flexible sensor array with an e-PTFE/PFA/FEP multilayer microcavity structure, reducing film stiffness and enhancing pressure sensing performance, applicable in physiological monitoring and surgical scenarios.[36] Reproduced with permission from ref. 36. Copyright (2024) Wiley-VCH Verlag GmbH & Co. KGaA, Weinheim. b. Fiber filter based on TENG with an annular microcavity structure, enabling airflow-driven electrostatic particle capture for sustainable personal protection.[93] Reproduced with permission from ref. 93. Copyright (2025) Elsevier. c. A porous PDMS-based triboelectric sensor with a water-containing gradient microchannel structure, where liquid migration and "water bridge" formation enhance linearity and support 3D tactile and bending sensing.[94] Reproduced with permission from ref. 94. Copyright (2024) Springer Nature.

and efficient capture of submicron particles, demonstrating the role of microcavity structures in self-powered filtration systems.

Porous PDMS materials are frequently utilized in the construction of triboelectric microfluidic sensors. Qin *et al.* design a sensor based on a water-containing elastomer structure, employing gradient-distributed multi-stage microchannels to create a sandwich-like porous microcavity network (Fig. 11c).[94] The microcavity provides both liquid storage and flow paths, and when the sensor nears its compression limit, a "water bridge" forms through liquid extrusion, dynamically adjusting the internal electric field, achieving a wide linear detection range from 5 to 1240 kPa. The porous microcavity improves deformation adaptability and charge migration efficiency, enabling the device to perform three-dimensional tactile recognition and bending angle sensing, thereby expanding the application scope of triboelectric sensing.

The integration of electret and triboelectric microcavity structures highlights a convergent pathway toward self-powered, highly sensitive, and spatially adaptive sensing systems. Through the coupling of permanent charge retention, dynamic air gap modulation, and porous dielectric design, these approaches enable multimodal signal conversion across both contact and non-contact scenarios. Collectively, they demonstrate the synergistic advantages of microcavity-enhanced self-powered sensing technologies in the development of next-generation human–machine interfaces, intelligent wearables, and low-power biomedical diagnostics.

Acoustic sensing

Microcavity architectures play a pivotal role in acoustic energy harvesting and transduction. They effectively capture acoustic energy, augment sound pressure, and adjust the frequency response, thereby efficiently converting weak acoustic vibrations into readily measurable and processable electrical or optical outputs, thereby constituting an effective pathway to enhancing the sensitivity of acoustic sensing.

Chen *et al.* propose an acoustic sensor (Fig. 12a) based on GO/DNA aerogel.[52] This sensor capitalizes on the porous microcavity structure to detects faint acoustic vibrations with high sensitivity and converts them into measurable resistance changes. It delivers an effective response bandwidth of 300–4000 Hz and a sensitivity of 74.4 kPa^{-1}, exhibiting highly synchronized responses to animal sounds, human voices, and environmental noise. Zhong *et al.* propose a highly sensitive acoustic sensor (Fig. 12b) based on PI/GO foam.[95] This sensor converts the tiny vibration energy, produced by the repeated reflection of sound waves within porous microcavity, into electrical signals, enabling the identification of both biological and non-biological sounds *via* distinct peaks. Liu *et al.* propose a highly sensitive graphene-based Fabry–Perot acoustic sensor (Fig. 12c).[96] By reducing the pressure change within the enlarged backing air cavity (EBC), the equivalent acoustic pressure acting on the diaphragm was increased, achieving an exceptionally high mechanical sensitivity of 187.32 nm Pa^{-1} @ 16 kHz. Active sensors require both a sound source and a sensor. Therefore, in terms of the sound

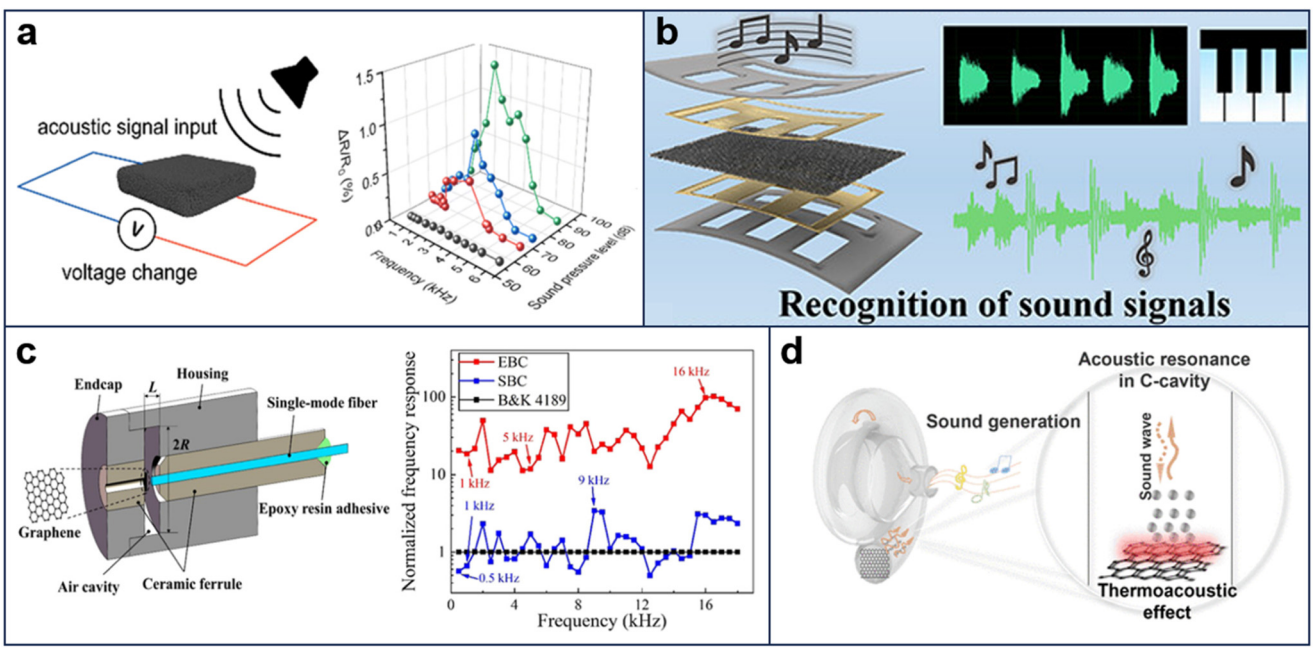

Fig. 12 Acoustic sensing systems and device architectures. a. Acoustic sensor based on GO/DNA aerogel.[52] Reproduced with permission from ref. 52. Copyright (2025) Royal Society of Chemistry. b. Highly sensitive acoustic sensor based on PI/GO foam.[95] Reproduced with permission from ref. 95. Copyright (2025) American Chemical Society. c. Graphene-based F–P acoustic sensor using the EBC.[96] Reproduced with permission from ref. 96. Copyright (2023) American Chemical Society. d. Wearable acoustic device based on graphene thermoacoustic resonator.[29] Reproduced with permission from ref. 29. Copyright (2025) AAAS.

source, Ren *et al.* report a wearable acoustic device based on graphene thermoacoustic resonance and a 3D-printed conch-inspired spiral cavity (Fig. 12d).[29] Tuning the cavity height affords control over the operating resonant frequency, yielding pronounced resonance enhancement at 5.4 kHz, with the sound pressure level (SPL) rising from 32 dB to 71 dB.

Brief summary. In summary, the incorporation of microcavity architectures drives measurable advances in high-sensitivity detection and broadband response within acoustic sensing, delivering strong performance in weak acoustic-signal detection, sound recognition, and HMI.

Other sensing

In addition to the aforementioned mainstream systems, microcavity-assisted sensing technologies based on optical and thermal principles also play a vital role in physical sensing within microfluidic systems. Fan *et al.* demonstrate an ultraviolet (UV)–near-infrared (NIR) dual-narrowband photodetector applicable to solar UV intensity monitoring and PPG signal detection (Fig. 13a).[97] By incorporating a microcavity structure, the device leverages optical interference effects to enhance its optical response at the resonant wavelength, allowing selective transmission of 330 nm UV light (transmittance >80%) while suppressing light in other spectral ranges. Zhu *et al.* report an organic PPG sensor that integrates a microcavity organic light-emitting diode (OLED) and an annular organic photodetector (OPD) (Fig. 13b).[63] By tuning the cavity length between the semi-transparent and reflective metal electrodes, the angular emission profile of the OLED is controlled, enhancing arterial light absorption, reducing baseline drift, and optimizing the pulsating signal. Movaghgharnezhad *et al.* design a highly sensitive broadband visible-light detection system based on a 3D heterogeneous multiscale porous graphene structure (Fig. 13c).[98] The interconnected multilevel porous microcavity improves photoresponsivity to 4.4 mA W^{-1}, representing a three-order-of-magnitude enhancement over monolayer graphene photodetectors. Li *et al.* propose a multifunctional phase-change aerogel for wearable thermal management (Fig. 13d).[99]

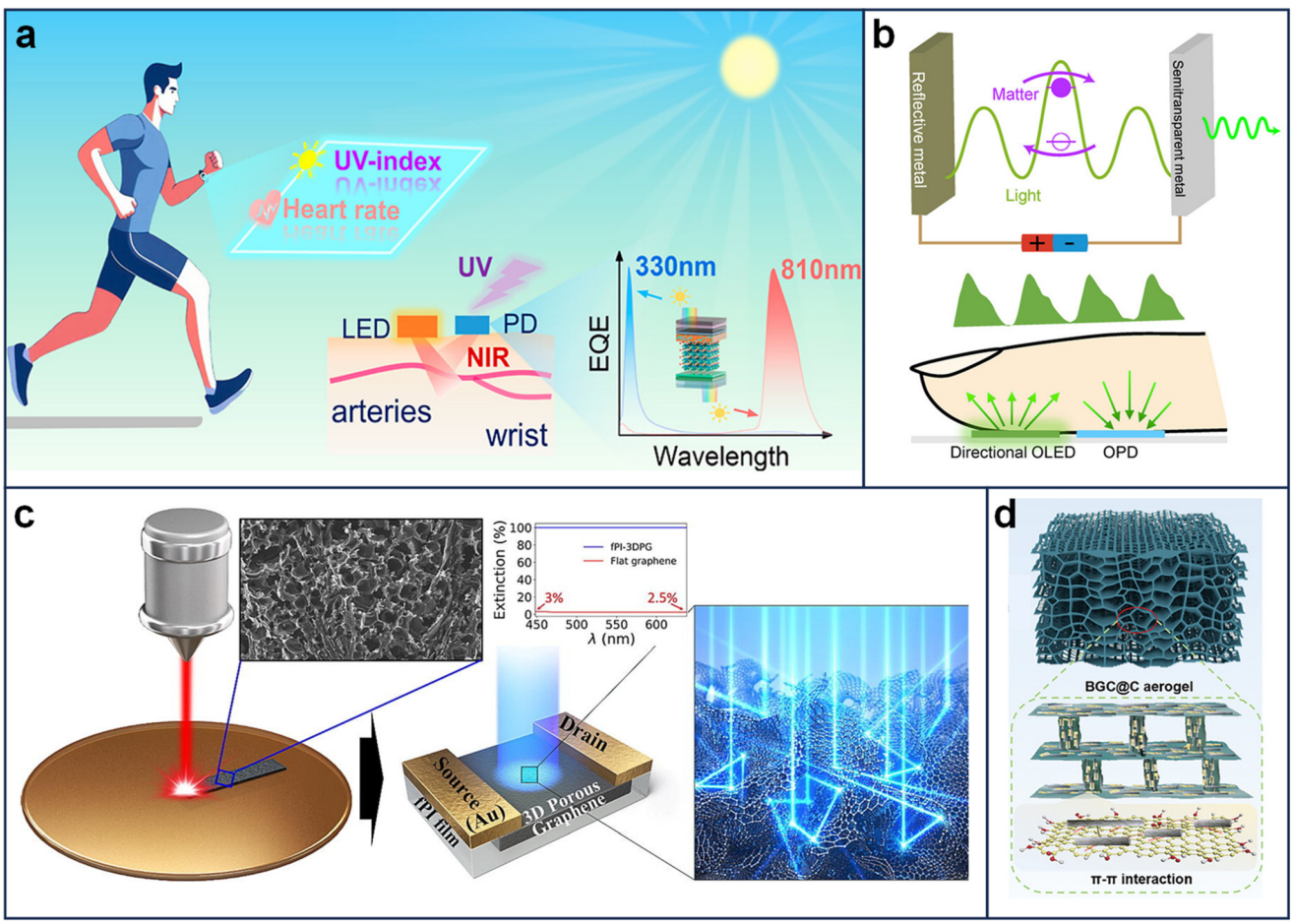

Fig. 13 Optical and thermal sensors. a. UV–NIR dual narrowband detector.[97] Reproduced with permission from ref. 97. Copyright (2025) American Chemical Society. b. An organic PPG sensor integrating a microcavity OLED and an annular OPD.[63] Reproduced with permission from ref. 63. Copyright (2024) Wiley-VCH GmbH. c. A high-sensitivity photodetector based on three-dimensional heterogeneous multiscale porous graphene.[98] Reproduced with permission from ref. 98. Copyright (2023) Elsevier. d. A multifunctional phase-change aerogel featuring both aerogel properties and thermal regulation performance.[99] Reproduced with permission from ref. 99. Copyright (2024) Wiley-VCH GmbH.

Leveraging a cross-linked continuous skeleton and preserved porous cavity structure, the material enhances heat storage capacity while maintaining the intrinsic properties of aerogels, such as thermal insulation, adsorption, and mechanical flexibility. The resulting thermal conductivity reaches 29.6 mW m^{-1} K^{-1}.

Brief summary. As a critical element in multiphysical sensing platforms, microcavity structures demonstrate functional versatility and structural compatibility across diverse sensing mechanisms. From enclosed air cavities and LM microchannels in mechanical sensing, to resonant acoustic chambers, and interference-based photothermal structures, microcavities enhance systematic performance by modulating local field distributions and strengthening signal coupling effects, leading to improved sensitivity, dynamic range, and spatial resolution. Researchers advance microcavity sensors toward enhanced performance, energy efficiency, and multimodal integration through co-design of materials and structures, in combination with AI algorithms, micro/nanofabrication, and flexible encapsulation technologies. The continuous evolution of sensing mechanisms and structural designs discussed in this chapter illustrates that microcavities are gradually becoming a bridge between material properties and system integration.

Summary and Prospect

Microcavity-assisted microfluidic physical sensors expand the capabilities of flexible sensors in precise measurement and multimodal signal processing through sophisticated cavity design, rational combinations of various flexible materials, and fabrication techniques suitable for mass production. This work provides a comprehensive analysis of microcavity architectures in microfluidic physical sensors, focusing on material optimization, representative structural typologies, and mechanisms for multimodal sensing. Special attention is given to their role in enhancing performance across resistive, capacitive, and triboelectric channels, emphasizing the pivotal contributions of microcavities to signal amplification, strain modulation, and multimodal signal integration. By integrating functional materials, such as polymers, porous materials, LMs, and carbon-based nanomaterials, microcavity structures substantially improve the sensitivity and temporal responsiveness of sensors, while simultaneously conferring superior mechanical flexibility, environmental adaptability, and system-level integrability. These attributes position microcavity-enabled devices as promising candidates for applications in health diagnostics, interactive systems, and environmental monitoring.

In contrast to conventional sensing architectures, microfluidic platforms exhibit distinct advantages in the context of physical signal detection. On one hand, the enclosed and controllable channels and cavity structures provide a stable three-dimensional support environment for microcavity units, helping to confine deformation regions and improve response repeatability. On the other hand, the design flexibility of microfluidic channels and their ability to manipulate fluid media make them naturally compatible with materials, such as LMs[100] and porous gels,[101] thereby enhancing the sensor's dynamic response and adaptability to complex environments. Microfluidic systems inherently possess the capacity to precisely modulate and transmit a wide range of physical stimuli, including pressure,[102] acoustic signals,[103] temperature,[104] and fluidic cues,[105] thereby establishing a foundational infrastructure for integrated multiparametric sensing.

Although significant advancements have been achieved, microcavity-enabled microfluidic sensing platforms continue to encounter challenges. The stability and long-term reliability of microcavity structures still depend on further optimization of material systems and packaging processes. Moreover, scalable and standardized high-throughput fabrication techniques for large-area production remain underdeveloped, thereby constraining the widespread implementation of such sensors in industrial and clinical applications. In addition, the convergence of multimodal sensing and AI algorithms remains predominantly at the experimental validation phase, with few cases of mature, systematic deployment.

Future research may advance along three principal directions. At the materials level, research focuses on novel composite systems that exhibit stretchability, autonomous self-healing, self-powering capabilities, and responsiveness to multiple physical stimuli. Efforts also aim to enhance their environmental tolerance under extreme conditions, while incorporating biodegradable and biocompatible materials to address the specific requirements of wearable and implantable medical devices. From a manufacturing standpoint, integrating techniques, such as laser micromachining, 3D printing, and soft lithography with automated encapsulation enables high-throughput, standardized, and large-area production, while the processing precision still requires further improvement. Furthermore, the development of multi-material co-fabrication and programmable structural manufacturing strategies addresses the growing demand for personalized and adaptive sensing solutions. Additionally, integrating physics-based model with machine learning enables the parametric design and predictive performance evaluation of microcavity architectures, thereby accelerating device design workflows. Regarding application and system integration, advancing the deep convergence of microcavity sensing with AI algorithms and low-power wireless communication is essential. Custom optimization should be performed for diverse application scenarios, including healthcare, HMIs, environmental monitoring, and industrial diagnostics, while pursuing developments toward high-density sensor arrays, minimized inter-channel crosstalk, and enhanced spatial resolution. Such progress ultimately facilitates the realization of multimodal, intelligent sensing architectures. Meanwhile, integrating physicochemical approaches is emphasized, wherein the inherent advantages of chemical sensing are harnessed in synergy with physical modalities to enable multimodal and multi-throughput data acquisition, thereby

supplying richer datasets to support algorithmic training and inference. For instance, hydrogels not only enable multimodal chemical sensing,[106] but are also commonly used in physical sensing applications.[38] By harnessing the material's capacity to adapt to diverse sensing mechanisms, it becomes possible to design multifunctional sensing systems. Similarly, by augmenting organ-on-a-chip platforms with physical sensing capabilities to monitor internal parameters, researchers can provide more effective guidance for experimental design and optimization.

Microcavity-assisted sensors possess a solid foundation for industrialization and strong potential for real-world deployment. In the field of wearable healthcare, the integration of enclosed microcavity structures and multimodal sensing algorithms enables noninvasive health assessments such as continuous blood pressure and pulse monitoring, applicable to smart health patches, postoperative rehabilitation monitoring, and chronic disease management systems.[107,108] In HMI and intelligent interfaces, structures involving porous electrets and LM microchannels are widely applicable in non-contact operating systems, AI-based interactive platforms, and tactile sensors for soft robotic end-effectors.[109–114] The incorporation of AI accelerates the advancement of microcavity sensor technologies. By using machine learning and computational modeling, researchers systematically explore material combinations and cavity designs with enhanced efficiency, thus reducing the research cycle; simultaneously, intelligent algorithms at the application-level function to integrate multimodal signals and discern complex patterns, which in turn enhances support for health monitoring and HMI. As demand grows for precise monitoring of controlled microenvironments, these systems can be further extended to applications in environmental sensing and microscale fluidic regulation. In extreme condition sensing, advanced materials including graphene aerogels and microstructured conductive foams enable precise detection in challenging settings involving high or low temperatures and high pressures.[115] Combined with scalable fabrication techniques such as soft lithography and 3D printing, it is expected to establish low-cost, mass-producible industrial platforms to support the rapid development of flexible electronics and digital healthcare.[116]

As research progresses, the focus of microcavity-assisted microfluidic physical sensors shifts from single performance optimization to more complex system integration and engineering applications. In the future, with the continuous progress of materials, fabrication processes, and intelligent algorithms, microcavity-assisted microfluidic sensing technology is expected to continue playing a role in intelligent perception systems and become a key technological enabler in fields of biomedicine, flexible electronics, and novel HMI.

Author contributions

Jianhua Zhou contributed to the conceptualization and funding acquisition for the project. He played a crucial role in project administration and supervision, and contributed to the review and editing of the manuscript. Yancong Qiao was responsible for the conceptualization of the study, overseeing the project administration and supervision. He also contributed significantly to writing and reviewing the manuscript. Xinyi Qu led the investigation process and was primarily responsible for writing the original draft. She contributed to the visualization of the study, and participated in the conceptualization of the study. Jianfeng Ma was involved in the investigation phase of the study and made contributions to the visualization aspects, including data representation and graphical elements. Degong Zeng contributed to the investigation phase, providing valuable input in the research process. He also helped with the review and editing of the manuscript. Jinan Luo was involved in the investigation and participated in the review and editing process of the manuscript. Jingzhi Wu, Chuting Liu, Zhikang Deng, Lvjie Chen, and Rongkuan Han: these authors contributed to the review and editing of the manuscript, providing insightful feedback and revisions to improve clarity, structure, and consistency, ensuring the final version met academic standards.

Conflicts of interest

There are no conflicts to declare.

Data availability

No primary research data, software, or code are generated or analyzed in this study. All data supporting this review are from previously published sources, which are cited within the article.

Acknowledgements

This work is supported by National Natural Science Foundation of China (No. 62201624, 32000939, 21775168, 22174167, 51861145202, U20A20168, 12302119), Shenzhen Medical Research Fund (No. A2403041), the Guangdong Basic and Applied Basic Research Foundation (No. 2024A1515012056; 2019A1515111183), Shenzhen Science and Technology Program (No. RCBS20221008093310024, JCYJ20230807111120043, RCBS20210706092407002; JCYJ20220818102014028), the Research Funds from Sun Yat-sen University (No. 2024_76200_B25890), the Fundamental Research Funds for the Central Universities, Sun Yat-sen University (No. 24xkjc034). The authors are also thankful for the support from Key Laboratory of Sensing Technology and Biomedical Instruments of Guangdong Province (No. 2020B1212060077).

References

1 S. Li, Y. Zhang, J. Liu, X. Wang, C. Qian, J. Wang, L. Wu, C. Dai, H. Yuan, C. Wan, J. Li, W. Du, X. Feng, Y. Li, P. Chen and B. Liu, *Small*, 2024, **20**, 2401848.
2 S. R. Little, Z. Leung, A. B. V. Quach, A. Hirukawa, F. Gholizadeh, M. Hajiaghayi, P. J. Darlington and S. C. C. Shih, *Adv. Mater. Technol.*, 2023, **8**, 2300719.

3 Y. Xie, L. Xu, J. Zhang, C. Zhang, Y. Hu, Z. Zhang, G. Chen, S. Qi, X. Xu, J. Wang, W. Ren, J. Lin and A. Wu, *Mater. Horiz.*, 2024, **11**, 5752–5767.
4 J. S. Y. Low, H. F. Teh, T. M. Thevarajah, S. W. Chang and S. M. Khor, *Biosens. Bioelectron.*, 2025, **270**, 116949.
5 W. Qiu and S. Nagl, *ACS Sens.*, 2021, **6**, 1147–1156.
6 Z. Zhu, S. Li, D. Wu, H. Ren, C. Ni, C. Wang, N. Xiang and Z. Ni, *Lab Chip*, 2022, **22**, 2097–2106.
7 A. Bhusal, E. Dogan, H.-A. Nguyen, O. Labutina, D. Nieto, A. Khademhosseini and A. K. Miri, *Biofabrication*, 2022, **14**, 014103.
8 Z. Yang, Z. Zhou, T. Si, Z. Zhou, L. Zhou, Y. R. Chin, L. Zhang, X. Guan and M. Yang, *Small*, 2023, **19**, 2207194.
9 X. Xiang, F. Li, Q. Ye, Y. Shang, M. Chen, J. Zhang, B. Zhou, H. Suo, Y. Ding and Q. Wu, *Sens. Actuators, B*, 2022, **358**, 131517.
10 X. Liu, Y. Wang, Y. Du, J. Zhang, Y. Wang, Y. Xue, J. Zhao, L. Ge, L. Yang and F. Li, *Chem. Eng. J.*, 2024, **486**, 150233.
11 X. Tong, X. Lin, N. Duan, Z. Lv, Z. Wang and S. Wu, *Sens. Actuators, B*, 2023, **397**, 134691.
12 Z. He, J. Huang, W. Shen, X. Lei, Y. Zhang, L. Zhu, X. Shen, D. Zhang, D. Yu and M. Zhou, *ACS Appl. Mater. Interfaces*, 2023, **15**, 24913–24922.
13 X. Zhao, Y. He, S. Shao, Q. Ci, L. Chen, X. Lu, Q. Liu and J. Chen, *ACS Sens.*, 2024, **9**, 2413–2420.
14 S. Pan, T. Zhang, C. Zhang, N. Liao, M. Zhang and T. Zhao, *Lab Chip*, 2024, **24**, 1668–1675.
15 Y. Luo, H. Fan, X. Lai, Z. Zeng, X. Lan, P. Lin, L. Tang, W. Wang, Y. Chen and Y. Tang, *Biosens. Bioelectron.*, 2024, **246**, 115905.
16 C. Zhang, J. Chen, C. Xu, T. He, X. Zhang, J. Zhang, X. Sun, B. Xu, Y. Zhu and H. Yang, *Nat. Commun.*, 2025, **16**, 1404.
17 M. Yuan, Z. Liu, X. Wu, H. Gou, Y. Zhang, X. Ning, W. Li, Z. Yao, Y. Wang, W. Pei and H. Chen, *Sens. Actuators, A*, 2023, **354**, 114250.
18 J. Li, L. Bo, T. Li, P. Zhao, Y. Du, B. Cai, L. Shen, W. Sun, W. Zhou and Z. Tian, *Adv. Mater. Technol.*, 2024, **9**, 2400572.
19 Y. Zheng, J. Sun, Y. Ma, H. Zhang, Z. Cui, G. G. Paschos, X. Song, Y. Tao, P. Savvidis, W. Kong, L. Wen, S. Bian and M. Sawan, *Adv. Sci.*, 2025, **12**, 2410125.
20 M. Wagih, J. Shi, M. Li, A. Komolafe, T. Whittaker, J. Schneider, S. Kumar, W. Whittow and S. Beeby, *Nat. Commun.*, 2024, **15**, 452.
21 R. You, Q. Fan, Z. Wang, W. Xing, Y. Wang, Y. Song, X. Duan, R. You and Y. Wang, *Research*, 2024, **7**, 0314.
22 A. M. Moran, V. T. Vo, K. J. McDonald, P. Sultania, E. Langenbrunner, J. H. V. Chong, A. Naik, L. Kinnicutt, J. Li and T. Ranzani, *Commun. Eng.*, 2024, **3**, 117.
23 X. Li, T. Chen, Z. Zheng, J. Gao, Y. Wu, X. Wu, T. Jiang, Z. Zhu and R. X. Xu, *Small*, 2024, **20**, 2404952.
24 P. Lemke, L. Schneider, W. Kunz, A. L. Rieck, P. S. Jäger, A. Bruckmann, B. Nestler, K. S. Rabe and C. M. Niemeyer, *Adv. Funct. Mater.*, 2024, **34**, 2313944.
25 K. J. Vahala, *Nature*, 2003, **424**, 839–846.
26 M. K. Zalalutdinov, J. T. Robinson, J. J. Fonseca, S. W. LaGasse, T. Pandey, L. R. Lindsay, T. L. Reinecke, D. M. Photiadis, J. C. Culbertson, C. D. Cress and B. H. Houston, *Nat. Commun.*, 2021, **12**, 3267.
27 X. Wang, G. Wu, X. Zhang, F. Lv, Z. Yang, X. Nan, Z. Zhang, C. Xue, H. Cheng and L. Gao, *Adv. Mater.*, 2025, **37**, 2410312.
28 H. L. Wang, T. Chen, B. Zhang, G. Wang, X. Yang, K. Wu and Y. Wang, *Small*, 2023, **19**, 2206830.
29 Y.-H. Wei, Z.-F. Guo, Y.-F. Wang, T. Lin, W.-W. Hou, S.-W. Duan, L.-Q. Tao, H. Tian, Y. Yang and T.-L. Ren, *Sci. Adv.*, 2025, **11**, eadv2801.
30 S. Dong, G. Ma, Z. Xiong, D. Ge, Y. Guo, W. Li and S. Zhang, *Adv. Intell. Syst.*, 2025, **7**, 2401019.
31 Z. Zhao, X. Zou, J. Zhang and K. W. C. Lai, *Adv. Electron. Mater.*, 2025, **11**, 2500124.
32 S. Xu, X. Guan, K. Bian, Q. Zhu, N. Dai, X. Zhao, Y. Qiu, S. Zheng, Y. Dong, J. Zhong, Q. Zhong and T. Hu, *Nano Energy*, 2024, **125**, 109553.
33 Y. Zhao, Q. Sun, S. Mei, L. Gao, X. Zhang, Z. Yang, X. Nan, H. Zhang, C. Xue and J. Li, *Microsyst. Nanoeng.*, 2024, **10**, 77.
34 M. S. Rahman, A. Shon, R. Joseph, A. Pavlov, A. Stefanov, M. Namkoong, H. Guo, D. Bui, R. Master, A. Sharma, J. Lee, M. Rivas, A. Elati, Y. Jones-Hall, F. Zhao, H. Park, M. A. Hook and L. Tian, *Sci. Adv.*, 2025, **11**, eads4415.
35 J. Luo, J. Wu, X. Zheng, H. Xiong, L. Lin, C. Liu, H. Liu, H. Tang, H. Liu, F. Han, Z. Liu, Z. Deng, C. Liu, T. Cui, B. Li, T.-L. Ren, J. Zhou and Y. Qiao, *Nano Res.*, 2024, **17**, 10058–10068.
36 L. Wu, J. Xue, J. Meng, B. Shi, W. Sun, E. Wang, M. Dong, X. Zheng, Y. Wu, Y. Li and Z. Li, *Adv. Funct. Mater.*, 2024, **34**, 2316712.
37 Q. Wu, C. Zhou, Y. Xu, S. Han, A. Chen, J. Zhang, Y. Chen, X. Yang, J. Huang and L. Guan, *ACS Sens.*, 2024, **9**, 2091–2100.
38 H. Wang, Q. Ding, Y. Luo, Z. Wu, J. Yu, H. Chen, Y. Zhou, H. Zhang, K. Tao, X. Chen, J. Fu and J. Wu, *Adv. Mater.*, 2024, **36**, 2309868.
39 N. Dai, X. Guan, C. Lu, K. Zhang, S. Xu, I. M. Lei, G. Li, Q. Zhong, P. Fang and J. Zhong, *ACS Nano*, 2023, **17**, 24814–24825.
40 H. Yang, X. Cao, Z.-G. Hu, Y. Gao, Y. Lei, M. Wang, Z. Zuo, X. Xu and B.-B. Li, *Photonics Res.*, 2023, **11**, 1139–1147.
41 G. Mogli, M. Costantini and S. Stassi, *Sens. Actuators, A*, 2025, **392**, 116734.
42 J. Liao, X. Dai, J. Han, J. Yang, Y. Wu, Y. Cao, Y. Qiu, Y. Wang, L.-B. Huang, H. Ni and W. Feng, *Nano Energy*, 2024, **121**, 109252.
43 J. Zhang, S. Wei, C. Liu, C. Shang, Z. He, Y. Duan and Z. Peng, *Microsyst. Nanoeng.*, 2024, **10**, 19.
44 D. Guo, X. Lei, H. Chen, L. Yi, Y. Li, Y. Zhao, F. Liu and G. J. Cheng, *Adv. Sens. Res.*, 2024, **3**, 2300165.
45 L. Liu, J. Li, Z. Tian, X. Hu, H. Wu, X. Chen, L. Zhang and W. Ou-Yang, *Nano Energy*, 2024, **128**, 109817.
46 H. Li, C. Zhang, H. Xu, Q. Yang, Z. Luo, C. Li, L. Kai, Y. Meng, J. Zhang, J. Liang and F. Chen, *Adv. Sci.*, 2025, **12**, 2413233.

47 J. Xu, Z. Wang, X. Wang, Y. Wu, R. Xing, T. Yu, Y. Li, J. Ao, Y. Tao, B. Bai, M. D. Dickey, D. Zhang and J. Yang, *Adv. Mater. Technol.*, 2023, **8**, 2201193.
48 L. Qin, W. Xia, Y. Wu, X. Huang, A. Nsilani Kouediatouka, H. Li, M. Ding, F. J. Mawignon, S. Lu, K. Cao, P. Yang, Y. Zhang and G. Dong, *ACS Appl. Mater. Interfaces*, 2024, **16**, 58980–58990.
49 Y. Li, B. Liu, P. Xu, J. Liu, X. Dai, A. Yu, T. Wang, L. Guo, T. Guan, L. Song and M. Xu, *Nano Res.*, 2024, **17**, 10008–10016.
50 Y. Qiu, Z. Zou, Z. Zou, N. K. Setiawan, K. V. Dikshit, G. Whiting, F. Yang, W. Zhang, J. Lu, B. Zhong, H. Wu and J. Xiao, *npj Flexible Electron.*, 2023, **7**, 37.
51 W. Hou, Y. Wei, Y. Wang, S. Duan, Z. Guo, H. Tian, Y. Yang and T.-L. Ren, *ACS Appl. Mater. Interfaces*, 2024, **16**, 23544–23552.
52 S. Chen, P. Zhang, J. Zhao, K. S. Novoselov and D. V. Andreeva, *Nanoscale Horiz.*, 2025, **10**, 1405–1413.
53 Y. Dai, Y. Li, S. Xuan, Y. Dai, T. Xu and H. Yu, *ACS Appl. Mater. Interfaces*, 2025, **17**, 11117–11125.
54 G. Yang, X. Zhang, R. Wang, X. Liu, J. Zhang, L. Zong and H. Yang, *Mater. Horiz.*, 2023, **10**, 1865–1874.
55 K. Bae, M. Kim, S. Sim, Y. Kang and J. Kim, *Small Methods*, 2025, **9**, 2401730.
56 J. Xu, G. S. Wood, E. Mastropaolo, P. Lomax, M. Newton and R. Cheung, *Micromachines*, 2023, **14**, 810.
57 Z. Zhu and X. Wang, *IEEE Sens. J.*, 2024, **24**, 8712–8720.
58 S. Zhang, B. Dong, Z. Wang, Z. Chen, T. Wei, J. Zheng and P. Lin, *ACS Appl. Electron. Mater.*, 2024, **6**, 7439–7447.
59 K. Tou, K. Nara, T. Sekine, Y. Wang, Y. Takeda, D. Kumaki and S. Tokito, *Adv. Sens. Res.*, 2023, **2**, 2300045.
60 I. Jeerapan, Y. Nedellec and S. Cosnier, *Nanomaterials*, 2024, **14**, 545.
61 J. Li, H. Jia, J. Zhou, X. Huang, L. Xu, S. Jia, Z. Gao, K. Yao, D. Li, B. Zhang, Y. Liu, Y. Huang, Y. Hu, G. Zhao, Z. Xu, J. Li, C. K. Yiu, Y. Gao, M. Wu, Y. Jiao, Q. Zhang, X. Tai, R. H. Chan, Y. Zhang, X. Ma and X. Yu, *Nat. Commun.*, 2023, **14**, 5009.
62 Z. Yang, J. Wang, X. Wan, H. Xu, C. Zhang, X. Lu, W. Jing, C. Guo and X. Wei, *Microsyst. Nanoeng.*, 2024, **10**, 177.
63 H. Zhu, H. Yu, J. Zhang, Y. Zhang, L. Zhang, S. Liu and W. Xie, *Laser Photonics Rev.*, 2024, **18**, 2400042.
64 X. Li, Y. Du, X. Pan, C. Xiao, X. Ding, K. Zheng, X. Liu, L. Chen, Y. Gong, M. Xue, X. Tian and X. Zhang, *Adv. Mater.*, 2025, **37**, 2416991.
65 J.-R. Zhang, A. Li, X.-L. Li, Y.-B. Zhao, J.-S. Sun, X.-X. Guo, W. Wang, J. Liu, Y.-L. Zhang and D.-D. Han, *ACS Appl. Mater. Interfaces*, 2025, **17**, 18940–18953.
66 Y. Zhang, H. Duan, G. Li, M. Peng, X. Ma, M. Li and S. Yan, *J. Nanobiotechnol.*, 2022, **20**, 246.
67 Y. Liu, C. Zhang, Y. Chen, R. Yin, P. He and W. Zhao, *ACS Appl. Mater. Interfaces*, 2023, **15**, 38572–38580.
68 F. Schneider, T. Fellner, J. Wilde and U. Wallrabe, *J. Micromech. Microeng.*, 2008, **18**, 065008.
69 W. Wang, G. Ren, M. Zhou and W. Deng, *Polymer*, 2021, **13**, 1075.
70 E. R. Cholleti, J. Stringer, M. Assadian, V. Battmann, C. Bowen and K. Aw, *Sensors*, 2018, **19**, 42.
71 M. C. Lopes, V. G. De Castro, L. M. Seara, V. P. A. Diniz, R. L. Lavall and G. G. Silva, *J. Appl. Polym. Sci.*, 2014, **131**, 41207.
72 H. J. Zo, S. H. Joo, T. Kim, P. S. Seo, J. H. Kim and J. S. Park, *Fibers Polym.*, 2014, **15**, 1071–1077.
73 D. Ding, Z. Shang, X. Zhang, X. Lei, Z. Liu, Q. Zhang and Y. Chen, *Ceram. Int.*, 2020, **46**, 28363–28372.
74 W. Zhang, L. Wang, S. Liu, F. Guan, M. Jiang, Y. Li, D. Yue, J. Li, X. Liu and Y. Feng, *J. Alloys Compd.*, 2023, **950**, 169760.
75 H. Li, X. Wang, Z. Ding, W. Gao, Y. Liu, K. Ma, Z. Hu and Y. Wang, *Polymers*, 2024, **16**, 1188.
76 B. A. Alshammari, M. Hossain, A. M. Alenad, A. G. Alharbi and B. M. AlOtaibi, *Polymers*, 2022, **14**, 1718.
77 P. Yang, F. Tian and Y. Ohki, *IEEE Trans. Dielectr. Electr. Insul.*, 2014, **21**, 2310–2317.
78 N. Jain, V. K. Singh and S. Chauhan, *J. Mech. Behav. Mater.*, 2017, **26**, 213–222.
79 K. S. Ramadan, D. Sameoto and S. Evoy, *Smart Mater. Struct.*, 2014, **23**, 033001.
80 M. A. H. Khondoker and D. Sameoto, *Smart Mater. Struct.*, 2016, **25**, 093001.
81 Y. Qiao, G. Gou, F. Wu, J. Jian, X. Li, T. Hirtz, Y. Zhao, Y. Zhi, F. Wang, H. Tian, Y. Yang and T.-L. Ren, *ACS Nano*, 2020, **14**, 3779–3804.
82 S.-Y. Yue, T. Ouyang and M. Hu, *Sci. Rep.*, 2015, **5**, 15440.
83 A. T. Khan, N. Wei, O. Salmela, K. Mustonen, Y. Liao, A. Hussain, E.-X. Ding, M. G. Uddin, H. Jiang, Y. Ohno and E. I. Kauppinen, *Carbon*, 2025, **239**, 120320.
84 A. Peigney, Ch. Laurent, E. Flahaut, R. R. Bacsa and A. Rousset, *Carbon*, 2001, **39**, 507–514.
85 R. Singampalli, R. Dachepalli, K. Chandra, B. Naidu, S. K. Nagasamudram, K. Srinivas, B. Basha and C. Beera, *Biointerface Res. Appl. Chem.*, 2019, **9**, 4205–4216.
86 Y. Yue, *ACS Appl. Eng. Mater.*, 2024, **2**, 638–648.
87 S. Ghosh, N. Kumar and S. Chattopadhyay, *Asian J. Pharm. Sci.*, 2025, **20**, 101007.
88 Y. Cao, P. Li, Y. Zhu, Z. Wang, N. Tang, Z. Li, B. Cheng, F. Wang, T. Chen and L. Sun, *ACS Sens.*, 2025, **10**, 272–282.
89 Y. Wu, S. Li, Z. Zhao, D. Zhang, X. Xiong, T. Yu, M. D. Dickey and J. Yang, *IEEE Sens. J.*, 2023, **23**, 9176–9182.
90 O. Gul, J. Kim, K. Kim, H. J. Kim and I. Park, *Adv. Mater. Technol.*, 2024, **9**, 2302134.
91 Y. Zhang, Q. Lu, J. He, Z. Huo, R. Zhou, X. Han, M. Jia, C. Pan, Z. L. Wang and J. Zhai, *Nat. Commun.*, 2023, **14**, 1252.
92 J. Liu, Y. Chen, Y. Liu, C. Wu, Z. Li, Y. Gao, X. Qiu, Y. Wang, X. Guo and F. Xuan, *ACS Appl. Mater. Interfaces*, 2024, **16**, 29188–29197.
93 G. Zhou, Y. Ma, B. Wei, J. Chen, Y. Zhang, S. Hu, J. Li and Y. Wang, *J. Colloid Interface Sci.*, 2025, **696**, 137871.
94 S. Qin, P. Yang, Z. Liu, J. Hu, N. Li, L. Ding and X. Chen, *Nat. Commun.*, 2024, **15**, 10640.
95 Y. Zhong, Y. Wang, L. Ma, P. He, J. Qin, J. Gao and J. Li, *ACS Appl. Mater. Interfaces*, 2025, **17**, 11154–11163.

96 Y. Liu, C. Li, B. Li, S. Lu, S. Fan, S. Dong, Z. Wan and M. Shen, *ACS Appl. Mater. Interfaces*, 2023, **15**, 51390–51398.
97 Q. Fan, K. Li, H. Zhang, C. Han, Z. Wang, Q. Li, Z. Wan, Y. Zhou, X. Liu and J. Huang, *ACS Photonics*, 2025, **12**, 1084–1094.
98 S. Movaghgharnezhad, M. Kim, S. Min Lee, H. Jeong, H. Kim, B. Gak Kim and P. Kang, *Mater. Des.*, 2023, **231**, 112019.
99 Y. Li, X. Zhao, Y. Tang, X. Zuo and H. Yang, *Adv. Funct. Mater.*, 2024, **34**, 2403059.
100 L. Dai, X. Wu, H. Hou, Z. Hu, Y. Lin and Z. Yuan, *Lab Chip*, 2024, **24**, 1977–1986.
101 C. Shen, H. Yang, W. She and Q. Meng, *Biotechnol. Bioeng.*, 2023, **120**, 2027–2038.
102 Y. Bai, X. Yu, X. Han, Y. Liu and G. Li, *Sens. Actuators, A*, 2024, **377**, 115683.
103 Y. Gao, T. Voglhuber-Brunnmaier, Y. Li, L. Akh, N. H. Patino, A. K. Fajrial, M. Ruzzene, B. Jakoby and X. Ding, *Phys. Rev. Lett.*, 2025, **134**, 037002.
104 Z. Huang, T. Chen, Y. Jiang, R. Zhou, Y. Wang, J. Ji, H. Xie, T. Pan, D. Fan, L. Liang, L. Yang, B. Jiang, P. Li, M. Gao, J. Zhu, G. Yao, D. Xue and Y. Lin, *npj Flexible Electron.*, 2025, **9**, 52.
105 F. Pappalardo, C. Panarello, S. Quattropani, L. Galluccio, A. Licciardello, R. Ruffino, G. Li-Destri, A. Lombardo, G. Morabito and N. Tuccitto, *Lab Chip*, 2025, **25**, 1707–1717.
106 Q. Ding, H. Wang, Y. Zhou, Z. Zhang, Y. Luo, Z. Wu, L. Yang, R. Xie, B. Yang, K. Tao, S. Pan, F. Liu, J. Fu, F. Huo and J. Wu, *Adv. Mater.*, 2025, **37**, 2502369.
107 P. Yi, X. Fu, Y. Liu, X. Zhang, C. Zhang and X. Li, *Nano Energy*, 2023, **113**, 108592.
108 K. Zhang, X. An, C. Wang, Y. Wang, Z. Sun, T. Ling, S. Lu and S. Sun, *J. Mater. Sci.*, 2025, **60**, 2419–2434.
109 Y. Pi, Q. Liu, Z. Li, D. Zhao, K. Zhang, Z. Liu, B. Zhou, I. M. Lei, Y. Ma and J. Zhong, *npj Flexible Electron.*, 2023, **7**, 45.
110 X. Wang, J. Lu, Y. Zhou, Y. Li, Z. Luo, Y. Gui, W. Lu and L. Li, *Adv. Funct. Mater.*, 2025, 2506305.
111 Q. Xie, L. Han, J. Liu, W. Zhang, L. Zhao, Y. Liu, Y. Chen, Y. Li, Q. Zhou, Y. Dong and X. Wang, *Adv. Healthcare Mater.*, 2025, **14**, 2402010.
112 X. Li, B. Qi, X. Wan, J. Zhang, W. Yang, Y. Xiao, F. Mao, K. Cai, L. Huang and J. Zhou, *Nano Energy*, 2023, **114**, 108652.
113 N. Li, F. Zhan, M. Guo, X. Yuan, X. Chen, Y. Li, G. Zhang, L. Wang and J. Liu, *Adv. Mater.*, 2025, **37**, 2419524.
114 G. Ye, Y. Yang, X. Zhang, Q. Wu, Y. Wan, N. Yang and P. Yang, *Adv. Funct. Mater.*, 2025, e10705.
115 Z. Li, X. Li, K. Pang, K. Li, Y. Gao, C. Zhang, J. Lu, Y. Liu, Z. Xu and C. Gao, *Nat. Commun.*, 2025, **16**, 6087.
116 S. Tisato, G. Vera, Q. Song, N. Nekoonam and D. Helmer, *Nat. Commun.*, 2025, **16**, 6730.